Developmental Biology 355 (2011) 286–301

Contents lists available at ScienceDirect

Developmental Biology

journal homepage: www.elsevier.com/developmentalbiology

The nucleolar GTP-binding proteins Gnl2 and nucleostemin are required for retinal neurogenesis in developing zebrafish

Judith T.M.L. Paridaen [1], Esther Janson [2], Kagistia Hana Utami, Tamara C. Pereboom, Paul B. Essers, Carina van Rooijen, Danica Zivkovic, Alyson W. MacInnes *

Hubrecht Institute for Developmental Biology and Stem Cell Research, Uppsalalaan 8, 3584 CT Utrecht, The Netherlands

ARTICLE INFO

Article history:
Received for publication 19 October 2010
Revised 18 April 2011
Accepted 21 April 2011
Available online 30 April 2011

Keywords:
Nucleolus
Retina
Neural differentiation
p53
Zebrafish

ABSTRACT

Nucleostemin (NS), a member of a family of nucleolar GTP-binding proteins, is highly expressed in proliferating cells such as stem and cancer cells and is involved in the control of cell cycle progression. Both depletion and overexpression of NS result in stabilization of the tumor suppressor p53 protein *in vitro*. Although it has been previously suggested that NS has p53-independent functions, these to date remain unknown. Here, we report two zebrafish mutants recovered from forward and reverse genetic screens that carry loss of function mutations in two members of this nucleolar protein family, Guanine nucleotide binding-protein-like 2 (Gnl2) and Gnl3/NS. We demonstrate that these proteins are required for correct timing of cell cycle exit and subsequent neural differentiation in the brain and retina. Concomitantly, we observe aberrant expression of the cell cycle regulators *cyclinD1* and *p57kip2*. Our models demonstrate that the loss of Gnl2 or NS induces p53 stabilization and p53-mediated apoptosis. However, the retinal differentiation defects are independent of p53 activation. Furthermore, this work demonstrates that Gnl2 and NS have both non-cell autonomously and cell-autonomous function in correct timing of cell cycle exit and neural differentiation. Finally, the data suggest that Gnl2 and NS affect cell cycle exit of neural progenitors by regulating the expression of cell cycle regulators independently of p53.

Introduction

During development, induction and progression of neuronal differentiation is a tightly regulated process that requires coordinated regulation of proliferation, cell cycle exit and cell fate decisions. In the developing vertebrate retina, six neuronal cell types (ganglion, amacrine, horizontal, bipolar, cone and rod photoreceptors) and one glial cell (Müller glia) type develop sequentially from a pool of apparently homogeneous multipotent precursors (reviewed by Harada et al., 2007). These particular cell types, their histology and anatomy, as well as the underlying circuitry of the eye are highly conserved in vertebrate species.

Gnl3/Nucleostemin (NS) was discovered as a nucleolar GTPase that is highly expressed in stem cells, cancer cells and other actively proliferating cells (Ma and Pederson, 2008; Tsai and McKay, 2002; Tsai and Meng, 2009). It belongs to a subfamily of YlqF/YawG GTPases that are characterized by a MMR1_HSR1 GTP-binding domain containing five circularly permutated GTP-binding motifs (Reynaud et al., 2005). Among members of the eukaryotic family of YlqF/YawG GTPases NS, Gnl3-like (Gnl3l), and Gnl2 (also known as NGP-1) are the most related (Reynaud et al., 2005; Tsai and Meng, 2009). Depending on their GTP-binding state, they shuttle between the nucleolus and the nucleoplasm, although their predominant localization is in the nucleolus (Meng et al., 2007; Tsai and McKay, 2005). Gnl2, which shares approximately 33% protein sequence homology with NS in humans, was initially identified as an immunoreactive autoantigen isolated from a breast tumor library (Racevskis et al., 1996). Similar to NS, Gnl2 shuttles between the nucleolus and the nucleoplasm (Meng et al., 2007). However, further functional characterizations of Gnl2 in vertebrates remain incomplete.

To date, vertebrate studies of NS have been limited to the observation that $Ns^{-/-}$ murine embryos are arrested at blastocyst stage due to a block in cell proliferation (Beekman et al., 2006; Zhu et al., 2006). NS has been shown to bind directly to the tumor suppressor p53 protein and depletion of NS results in p53 stabilization (Dai et al., 2008; Meng et al., 2008; Tsai and McKay, 2002). Under normal physiological conditions, p53 levels are kept low through the binding to the E3 ubiquitin ligase Mdm2. Under stress conditions induced by DNA damage, hypoxia, or oncogenic stress, Mdm2-mediated degradation of p53 is inhibited by the phosphorylation of p53 and decoupling from Mdm2 (Horn and Vousden, 2007). Stabilized p53

* Corresponding author. Fax: +31 30 2516 464.
E-mail addresses: e.janson@umcutrecht.nl (E. Janson), kagistiahu99@gis.a-star.edu.sg (K.H. Utami), t.pereboom@hubrecht.eu (T.C. Pereboom), p.essers@hubrecht.eu (P.B. Essers), c.vanrooijen@hubrecht.eu (C. van Rooijen), d.zivkovic@hubrecht.eu (D. Zivkovic), a.macinnes@hubrecht.eu (A.W. MacInnes).
[1] Present address: Max-Planck-Institute of Molecular Cell Biology and Genetics, Pfotenhauerstrasse 108, D-01307 Dresden, Germany.
[2] Present address: Department of Medical Genetics, University Medical Center Utrecht, Heidelberglaan 100, 3584 CG Utrecht, The Netherlands.

0012-1606/$ – see front matter © 2011 Elsevier Inc. All rights reserved.
doi:10.1016/j.ydbio.2011.04.028

subsequently mediates cell cycle arrest by inducing expression of target genes, including cell cycle inhibitors such as p21 (Riley et al., 2008). *In vitro* as well as *in vivo* knockdown of NS causes G1-S phase arrest and reduced cell proliferation (Beekman et al., 2006; Dai et al., 2008; Ma and Pederson, 2007; Tsai and McKay, 2002; Zhu et al., 2006). Additional *in vitro* knockdown of p53 reversed the reduction in cycling cells, showing that the cell cycle arrest is p53-dependent (Ma and Pederson, 2007). The p53-mediated G1 cell cycle arrest was proposed to result from enhanced binding of the ribosomal proteins rpL5 and rpL11 that are released from the nucleolus to Mdm2 in the cytoplasm (Dai et al., 2008). Recent studies have shown that in addition to G1-S phase arrest, NS knockdown also causes G2-M phase arrest *in vitro* that might also be p53-dependent (Meng et al., 2008; Zhu et al., 2006).

Initially, it was shown that overexpression of NS causes p53 stabilization by direct binding and inhibition of Mdm2 (Dai et al., 2008). Recent data, however, have shown that NS overexpression and forced relocalization of NS to the nucleoplasm results in stabilization of Mdm2 by inhibition of its degradation, which would subsequently inhibit p53 activity (Meng et al., 2008). These findings suggest a role for NS in controlling p53 activity in situations where NS would be localized in the nucleoplasm, such as upon nucleolar stress and during mitosis.

Several data suggest that not all defects following NS depletion or overexpression are linked to p53 activity. Additional depletion of functional p53 in $Ns^{-/-}$ murine embryos did not rescue the lethal phenotype caused by the loss of NS (Beekman et al., 2006). Also, combined *in vitro* knockdown of the ribosomal proteins rpL5, rpL11 and NS caused only a partial rescue of proliferation, despite the fact that p53 activity levels were returned to normal (Dai et al., 2008). These data suggest that further mechanisms of cell cycle control by NS remain to be elucidated.

Here, we analyze the consequences of zygotic-effect mutations in *gnl2* and *ns* on zebrafish development. We demonstrate that Gnl2 and NS function redundantly in retinal neurogenesis. Loss of Gnl2 or NS causes retinal progenitor cells to fail induction of cell cycle exit on time, which appears to be the result of aberrant expression of cell cycle regulators. In addition, differentiation of all retinal neural cell types is delayed and reduced. We show that the failure of *gnl2* and *ns* mutant retinal progenitors to differentiate is not due to p53-induced cell cycle arrest. In addition, we show that the function of *gnl2* and *ns* in retinal neurogenesis have both non-cell autonomous and cell-autonomous aspects. Altogether, our findings suggest a novel role of these nucleolar GTPases in maintaining proper levels of *cyclinD1* and *p57kip2* that are key regulators of cell cycle progression.

Material and methods

Zebrafish embryos and fish maintenance

Zebrafish embryos were raised and staged as previously described (Westerfield, 1995). The $gnl2^{bw41c}$ mutation was recovered in a forward genetic screen, whereas the ns^{hu3259} mutation was generated in a reverse genetic screen using the TILLING method (Wienholds and Plasterk, 2004). All mutant embryos were genotyped by nested PCR, followed by Taqa1 restriction and fragment length electrophoresis for *gnl2* and DNA sequencing for *ns* mutants, using the following primers: PCR1 gnl2-1 5′-ggtgcctgtctgttaatcaag-3′, gnl2-4 5′-gcgcta tacacgcatt-taac-3′; PCR2 gnl2-2 5′-ttacacatttgccacagacc-3′, gnl2-3 5′-tgcagcaaa-gacattggtag-3′ and PCR1 ns-1 5′-taggt caacattgcccaac-3′, ns-4 5′-gagagtatcaaacacatgcagag-3′; PCR2 ns-2 5′-tttctca ctattccaggttcg-3′, ns-3 5′-tgttgagttcttggcatt tg-3′.

Plasmid construction

pCS2 + MT-d-Gnl2 and pCS2 + MT-d-Ns constructs were constructed as follows. Full-length 2.2 kb Gnl2 (NM_213224) and 1.6 kb NS (NM_001002297) cDNAs were obtained by reverse transcription of 48 hpf WT zebrafish embryo-derived total RNA isolated in Trizol (Invitrogen, Carlsbad, CA), followed by PCR using Phusion proofreading Taq polymerase (Finnzyme, Espoo, Finland) according to the manufacturer's instructions. The primers used were: Gnl2-F 5′-ttgaat tcaaagatgttaagg-3′, Gnl2-R 5′-aactcgagttatcgcttggctcgatt-3′ and Ns-F 5′-ttgaattcag acatgaagagaccgaagttgaag-3′, Ns-R 5′-aactcgagttaca-caaagtctgtgtt-3′ that contained an EcoRI and XhoI restriction site, respectively. Subsequently, the PCR product was cloned into the EcoRI–XhoI sites of the pCS2 + MT expression vector. All constructs were verified by sequencing.

Western blotting

Embryos were untreated or exposed to 25 Gy of γ-irradiation. Four hours after irradiation embryos were lysed (5 embryos/sample) in Triton X-100 sample buffer, run over a 10% SDS-PAGE gel, transferred and blotted with a monoclonal anti-zebrafish p53 antibody as previously described (MacInnes et al., 2008) and actin antibody (Santa Cruz; sc-1616-R).

Microarray hybridization and analysis

As a control for embryo sorting efficiency with respect to phenotype–genotype correspondence, half of the collected *gnl2* mutant embryos were genotyped and the other half used for RNA isolation. Of the test-sorted collected embryos, 92% were genotypically $gnl2^{-/-}$ mutants (n = 75), with the remaining 8% consisting of $gnl2^{+/-}$ siblings.

Total RNA was isolated from 40 *gnl2* and 40 WT embryos at 22 hpf using Trizol (Invitrogen) according to the manufacturer's instructions. Subsequently, RNA quality was checked using capillary gel electrophoresis (BioAnalyzer, Agilent Technologies, Santa Clara, CA, USA). cDNA was generated using the low RNA input linear amplification kit and labeled with Cy3 or Cy5-CTP (Perkin-Elmer, Waltham, MA, USA). Upon purification using an RNeasy column (Qiagen) and fragmentation, labeled cRNA was hybridized to the zebrafish 22K 60-mer oligonucleotide microarray (G2518A-001, Agilent) at 60 ºC for 17 h. Subsequently, slides were scanned using a microarray slide scanner (Agilent).

Two independent biological repeats starting from independent total RNA isolations were performed. Genes with Fold-Change > 1.5, were selected and uploaded to Genetools (http://www.genetools.no) for gene ontology analysis according to the Gene Ontology category "biological process". The microarray data have been deposited in the National Center for Biotechnology Information's Gene Expression Omnibus and are accessible through GEO Series accession number GSE21134.

BrdU and EdU labeling of embryos

Dechorionated embryos were incubated in 10 mM BrdU (Sigma) or 400 μM EdU (Invitrogen) in 15% DMSO in embryo medium on ice for 30 min. Embryos were washed in fresh embryo medium and cultured for an additional 5 min before fixation in 4% paraformaldehyde.

Histology

For histological analysis, embryos were fixed in 4% PFA in phosphate buffer, dehydrated, embedded in plastic (Technovit), and sectioned at 7 μm. Subsequently, sections were stained in 1% toluidine blue for 1 min, mounted with Depex and coverslipped.

In situ hybridizations and immunohistochemistry

In situ hybridizations and immunohistochemistry were performed essentially as previously described (Diks et al., 2006). DIG-labeled riboprobes were synthesized according to the manufacturer's instructions (Roche): *ascl1a* (Allende and Weinberg, 1994), *ath5* (Masai et al., 2000), *irx1a* (Cheng et al., 2001). *gnl2* and *ns* probes were synthesized by direct riboprobe synthesis using T3 RNA polymerase on purified PCR products for *gnl2* exon 13 and *ns* exons 10 to 15 that were obtained using the following primers: Gnl2-exon13F 5′-taatacgactcactataggAGGCGATGCTGGAAATG, Gnl2-exon13R 5′-aattaaccctcactaaagggGGAGAAGTGCTTTGACTTGG-3′ and Ns-exon10-15F 5′-taatacgactcactataggCAACAGTGCAATCAGCAG-3′, Ns-exon10-15R 5′-aattaaccctcactaaagggGTCAGGTCAGTGTTGACTGG-3′. Probes to *ccnd1* (NM_131025) and *p57kip2/cdkn1c* (NM_001002040) were synthesized on PCR products using the following primers: Ccnd1-exon1/2F 5′-taatacgactcactatagg GACTCGAGCTCCAGCTTTC-3′, Ccnd1-exon1/2R 5′-aattaaccctcactaaagggAGGAA GTTGGTGAGGTTCTG-3′, and Cdkn1c-exon1F 5′-taatacgactcactataggAA ACAAACGTCGGCT-CAC-3′, Cdkn1c-exon1R 5′-aattaaccctcactaaagggGAGGACT GAAGAAC-GAGCTG-3′. As a template for PCR, cDNA was synthesized from 48 hpf zebrafish embryo-derived total RNA. All PCR products were verified by sequencing. Antibodies used were rat anti-BrdU (Sigma, 1:200), rabbit anti-PH3 (Upstate Biotechnology, Lake Placid, USA; 1:200), mouse anti-zn8 (ZIRC, 1:50), mouse anti-zrf1 (ZIRC, 1:1000), mouse anti-zpr1 (ZIRC, 1:10), mouse anti-glutamine synthase (Millipore, 1:2000), α-HuC/D (Molecular Probes, 1:200), followed by a Cy3-conjugated secondary antibody (Jackson ImmunoResearch, Suffolk, UK). For BrdU/PH3 double immunofluorescence, cryosections were prepared as follows: fixed embryos were incubated sequentially in 5 and 30% sucrose in PBS, followed by embedding and freezing in OCT medium (Sakura), and cryosectioning at 10 μm. Sections were permeabilized for 2 h in 100% methanol in −20 °C followed by a 30 min incubation in 0.2% Triton-X100 in PBS and a 30 min incubation in 2 N HCl to denaturate DNA. Before incubation in antibodies, sections were blocked for 1 h in 2% normal goat serum, 1% BSA, 1% DMSO in PBS. For EdU/Zn8 double immunofluorescence, embryos were permeabilized using proteinase K (Sigma), incubated in EdU detection mix (Click-iT EdU Alexa647 imaging kit,Invitrogen) for 1 h according to the manufacturer's instructions and washed with 3% BSA in PBS. Subsequently, embryos were processed for zn8 immunofluorescence. TUNEL assays were performed as described previously using TdT polymerase (Promega) and DIG-UTP (Roche) (Diks et al., 2006).

Microinjections

A translation-blocking morpholino oligonucleotide was designed to the ATG region of *gnl2* (5′-TCCCCTTGAATTTTGCCTTAACCAT-3′; Gene Tools, Philomath, OR) and 0.5 to 10 ng was injected into one-cell stage embryos using pulled glass micropipettes. One nanogram of p53 morpholino oligonucleotide (5′-GCGCCATTGCTTTGCAAGAATTG-3′; (Langheinrich et al., 2002)] Gene Tools, Philomath, OR) was injected into one-cell stage embryos. Capped mRNAs were synthesized using the mMESSAGE mMACHINE kit (Ambion). WT *gnl2* and *ns* mRNA was injected in a range of 400 to 500 pg into one-cell stage embryos.

Mosaic analysis

One-cell donor embryos were injected with 25 mg/ml mini-emerald (lysine-fixable dextran-fluorescein and -biotin 10,000 MW, D7178, Invitrogen). Ten to fifty cells of sphere-stage embryos were transplanted into the prospective eye field of shield-stage host embryos using an oil-filled pulled glass capillary connected to a micro-injector (Cell-Tram Vario, Eppendorf). Transplanted embryos were examined for location of transplanted cells and exposed to a 30-minute EdU pulse at 48 hpf and fixed. Transplanted cells were visualized by incubating embryos in streptavidin conjugated to Alexa488 (1:250, Invitrogen).

Imaging

In situ images were obtained using a Zeiss Axioplan Stereomicroscope (Oberkochen, Germany) equipped with a Leica (Wetzlar, Germany) digital camera. Fluorescent labelings were imaged using a Leica TCS SPE confocal microscope using 20× or 40× magnification or an Olympus Fluoview FV1000 using 20× magnification. Images were adjusted for brightness and contrast using Adobe PhotoshopCS2.

Quantifications

For analysis of retinal cryosections, cell numbers were quantified using ImageJ software (NIH) on two sections of the central retina of each animal using DAPI as a nuclear counterstain to determine total retinal cell number. For analysis of the transplantations, raw confocal stacks were imported into ImageJ and for each z-plane (z-step 2 μm), DAPI-stained nuclei, fluorescein+, EdU+ and Zn8+ cells were marked using the manual cell counter plug-in, taking care not to include duplications of same cells. Subsequently, the total number of each marked cell type was exported to Microsoft Excel to analyze the proportion of each cell type/transplanted clone. For analysis of the EdU distribution, clones of transplanted cells were divided into 6 equidistant bins along the apico-basal axis of the clone/retina. Subsequently, the number of EdU+ cells was determined for each bin. For EdU intensity analysis, raw confocal stacks were imported into ImageJ and a line drawn perpendicular to the apico-basal axis of the transplanted clone and immediate surroundings. Next, a plot profile was created for gray values along the line for EdU and fluorescein.

Statistics

For each experiment, the chosen method of statistical analysis and resulting p-values are stated in the text. Two-tailed Student's *t*-tests assuming significance levels of $\alpha = 0.05$ were performed using Microsoft Excel software; two-tailed Fisher's exact probability tests for a table of frequency data were performed online (http://faculty.vassar.edu).

Results

A mutation in gnl2 causes unscheduled neuronal differentiation in the zebrafish embryo

The *bw41c* zebrafish mutant was recovered in a forward mutagenesis screen (D.Z., unpublished data) as aberrant in early neuronal differentiation from 24 h post-fertilization (hpf). Expression of the basic helix–loop–helix (bHLH) transcription factor *achaete-scute complex-like 1a* (*ascl1a*; Figs. 1A–F) and other proneural genes (data not shown) was expanded. This was accompanied by premature terminal neuronal differentiation as visualized by the early post-mitotic neuronal marker HuC/D at 36 hpf (Figs. 1G and H).

Morphologically, *bw41c* mutants were distinguishable from wild-type (WT) embryos from 22 hpf by a reduced forebrain, expanded hypophysis, smaller eyes, a thinner mid/hindbrain boundary (MHB) and a hyperinflated hindbrain ventricle (Figs. 1I–L). At later stages, the *bw41c* mutant embryos showed a shorter and more curved body (Suppl. Fig. 1L). Homozygous embryos die around 5 days post-fertilization (dpf), whereas heterozygous embryos develop normally.

To identify the mutated gene, genetic mapping using chromosome-specific sequence length polymorphisms (SSLPs) and single nucleotide polymorphism (SNPs) (Guryev et al., 2006) was used to narrow

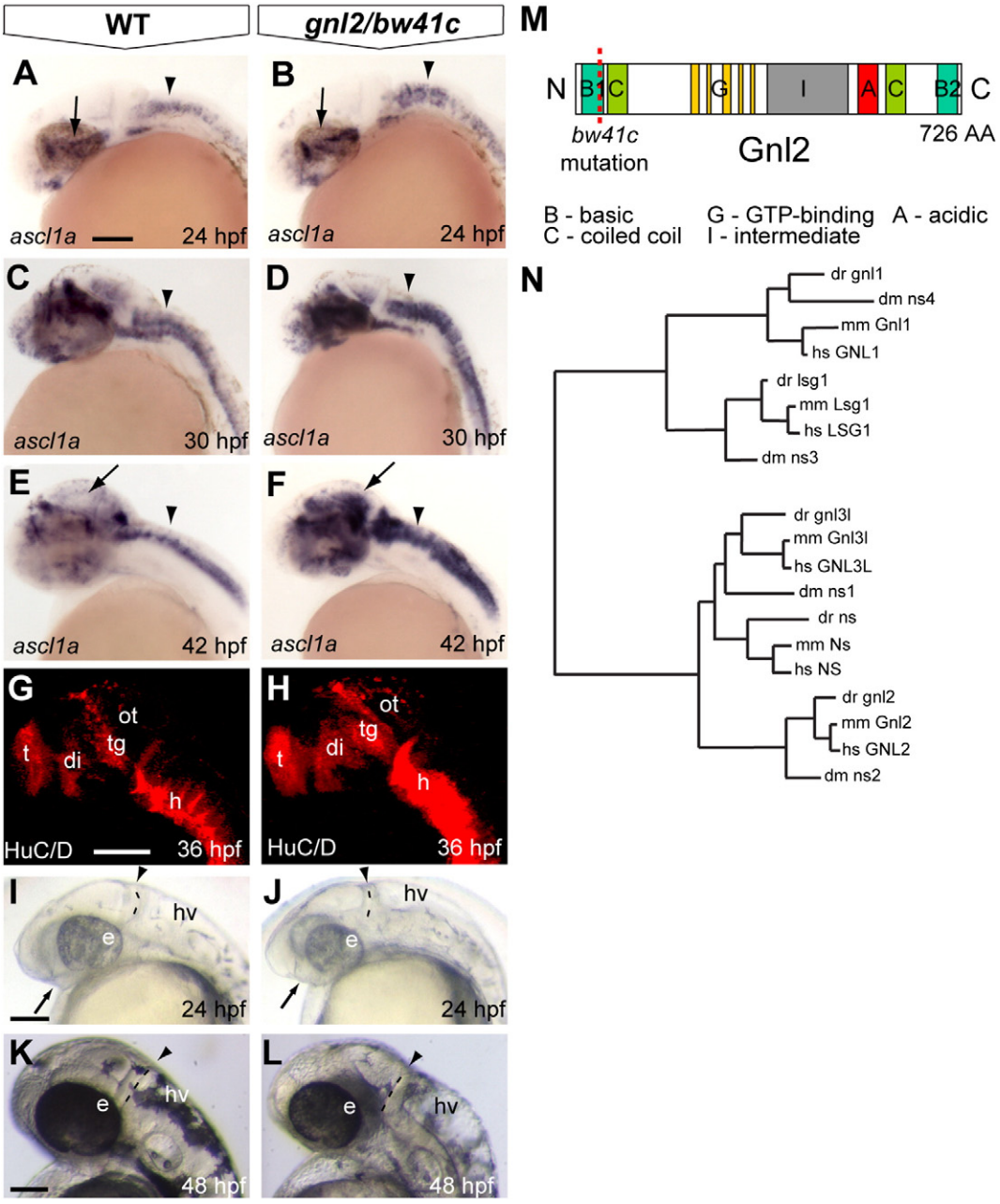

Fig. 1. Identification of a loss of function mutation in zebrafish *gnl2*. (A–F) Expression of the proneural bHLH transcription factor *ascl1a* is subtly expanded in the *bw41c* mutant (B) diencephalon (arrow) and hindbrain (arrowhead) at 24 hpf. At 30 hpf, the *ascl1a*-expressing domain is expanded in the *bw41c* mutant hindbrain (arrowhead in D). At 42 hpf, *ascl1a* expression is expanded in the midbrain (arrow), dorsal diencephalon and hindbrain (arrowhead) of *bw41c* mutants (F). (G and H) At 36 hpf, neuronal clusters were expanded in the *bw41c* mutant brain as demonstrated by the terminally differentiated neuronal marker HuC/D. (I–L) *bw41c* mutant phenotype at 24 (J) and 48 hpf (L). The earliest clearly visible defects in *bw41c* mutants (J) are the reduced forebrain (arrow), smaller eyes, thinner mid/hindbrain boundary (dashed line and arrowhead) and hyperinflated hindbrain ventricle. At 48 hpf, *bw41c* mutants (L) are characterized by smaller eyes, thinner mid/hindbrain boundary (dashed line and arrowhead) and severe hyperinflation of the hindbrain ventricle. (M) Schematic drawing of the Gnl2 protein with the *bw41c* mutation indicated by the dashed red line. (N) Phylogenetic tree of the five members of the Gnl family, Lsg-1, Gnl1, Gnl2, Gnl3/NS and Gnl3l in *Drosophila melanogaster* (dm), *Danio rerio* (dr), *Mus musculus* (mm) and *Homo sapiens* (hs). Lsg1 and Gnl1 on one hand, and Gnl2, Gnl3/NS and Gnl3l on the other hand appear to have separate common ancestors. In *Drosophila* and other invertebrates, there are no separate orthologs of Gnl3/NS and Gnl3l, but one common ortholog that is more similar to NS than to Gnl3l. All images are lateral view, with anterior to the left and dorsal up. di, diencephalon; e, eye; h, hindbrain; hv, hindbrain ventricle; ot, optic tectum; tg, tegmentum; t, telencephalon. Scalebar 125 μm.

down the candidate region to a ~356 kb region on chromosome 16 (Suppl. Fig. 1A). Sequencing of seven genes present in this region identified a cytosine to thymine mutation introducing a premature stop codon in exon 3 of *guanine nucleotide binding protein-like 2* (*gnl2*; Suppl. Fig. 1B), corresponding to an arginine in position 53 within the first basic domain of the zebrafish Gnl2 protein (Fig. 1M). Gnl2 is a member of a family of evolutionary conserved circularly permutated GTPases, among which Gnl3/Nucleostemin is the best known (Fig. 1N) (Ma and Pederson, 2008; Tsai and Meng, 2009). Since the *bw41c* mutation is located early in the protein and N-terminal to the GTP-binding sites (Fig. 1M), the mutation is predicted to result in a loss of function of Gnl2.

To confirm that the *bw41c* mutation leads to Gnl2 loss of function, we utilized a translation-blocking ATG-morpholino (MO) specific to the *gnl2* sequence. Indeed, injection of 2 to 10 ng of *gnl2* MO into WT embryos phenocopied the *bw41c* mutant phenotype (Suppl. Figs. 1D–K) as it resulted in expanded expression of proneural genes similar to the *bw41c* mutant.

Injection of a low dose of *gnl2* MO (0.5 ng), which mildly affected only 30% of injected *gnl2*$^{+/+}$ siblings (n = 10), severely exacerbated the *bw41c* phenotype in 82% of the injected *gnl2*$^{-/-}$ embryos (n = 11) and induced a *bw41c*-like phenotype in 53% of the injected *gnl2*$^{+/-}$ siblings (n = 17; data not shown). To further confirm that disruption of *gnl2* underlies the *bw41c* phenotype, WT *gnl2* mRNA was injected into progeny of *gnl2*$^{+/-}$ carriers. Injection of WT *gnl2* mRNA partially rescued the smaller eye and body size of *gnl2* mutants (Suppl. Fig. 1N). Injection of higher doses (>475 pg) of WT *gnl2* mRNA in WTs or *bw41c* mutants resulted in lethality. These data led us to conclude that Gnl2 loss of function is indeed the cause of the *bw41c* phenotype. The *bw41c*/*gnl2* mutant may be viewed as a hypomorph due to the presence of maternal mRNA and/or protein that masks potential earlier phenotypes.

A mutation of gnl3/nucleostemin results in phenotypes similar to the loss of gnl2

To understand more about the potentially important role of NS and related proteins such as Gnl2 in embryonic development, we set out to compare the NS loss of function phenotype in developing zebrafish with that of Gnl2. To achieve this, we employed the TILLING (Targeting Induced Local Lesions IN Genomes) method (Wienholds and Plasterk, 2004) to generate a nonsense mutation in the *ns* gene. We identified a nonsense mutant allele, *ns*^{hu3259}, which contained a premature stop codon in exon 5 of the zebrafish *ns* gene corresponding to a glutamic acid in position 117 (Suppl. Fig. 1C). The resulting phenotype (Figs. 2A–D) is reminiscent of the phenotype observed in the *ns*/*gnl3*^{hi299Tg} mutant allele generated by an independent viral integration screen (Amsterdam et al., 1999). This similarity and the fact that the *ns* mutation resides N-terminal to the GTP-binding domains of NS (Fig. 2E) suggest that the *ns* mutation represents an NS loss of function.

Similar to the *gnl2* mutant, homozygous *ns* mutants were morphologically distinct from WT siblings around 22 hpf and were characterized by a reduced forebrain, expanded epiphysis, reduced MHB and hyperinflated hindbrain ventricle (Figs. 2A and B). At later stages, *ns* mutants were generally smaller than their WT siblings, including smaller eyes and heads, although the body curvature, size reduction and age of lethality were all the more severe in the *gnl2* mutants (Figs. 2C and D, Suppl. Fig. 1M). Heterozygous *ns* embryos were phenotypically normal. To confirm that the *ns* phenotype is specifically due to a loss of NS, WT *ns* mRNA was injected into the progeny of *ns*$^{+/-}$ fish. Injection of 500 pg WT *ns* mRNA, but not of lower concentrations, partially rescued the embryo size, including eye size (Suppl. Fig. 1O). Injection of higher doses of *ns* mRNA caused lethality.

Gnl2 and NS have (partially) redundant functions

We examined *gnl2* and *ns* expression throughout development and found both genes to be expressed throughout the WT embryo, with high levels of expression in proliferating areas of the brain and

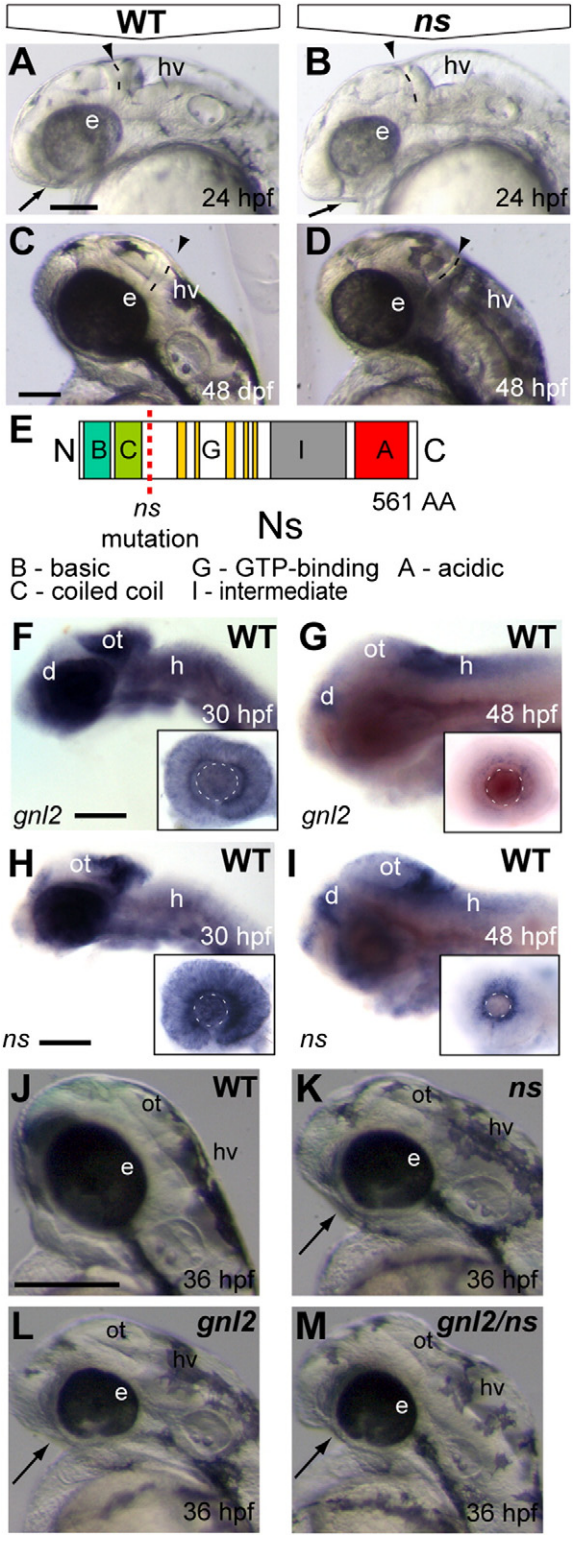

Fig. 2. A loss of function mutation in zebrafish *ns* indicates redundancy between Gnl2 and NS. (A–D) The earliest visible defects that emerge around 24 hpf (A and B) in *ns* mutants (B) are the reduced forebrain (arrow), reduced eye size, thinner mid/hindbrain boundary (dashed line and arrowhead) and hyperinflated hindbrain ventricle. At 48 hpf, *ns* mutants (D) are characterized by smaller eyes, thinner mid/hindbrain boundary (dashed line and arrowhead) and severe hyperinflation of the hindbrain ventricle. (E) Schematic drawing of the NS protein with the position of the *ns*^{hu3259} mutation indicated by the red dashed line. (F and G) *gnl2* transcript is expressed throughout the brain at 30 hpf (F), with higher expression levels in the dorsal diencephalon, optic tectum, hindbrain and retina (inset in F). At 48 hpf (G), *gnl2* transcript is expressed in the proliferative areas of the brain, namely the dorsal diencephalon, posterior optic tectum and hindbrain. In the retina, *gnl2* expression is restricted to the proliferative ciliary marginal zone at 48 hpf (inset in G). *ns* transcript is expressed throughout the brain at 30 hpf (H), with higher expression levels in the dorsal diencephalon, optic tectum, hindbrain and retina (inset in H). At 48 hpf, *ns* transcripts are expressed in the dorsal diencephalon, posterior optic tectum and hindbrain (I). In the retina, *ns* is expressed in the ciliary marginal zone (inset in I). (J–M) The morphology of WT (J), single *ns* (K), single *gnl2* (L) and *gnl2*/*ns* compound mutants (M) shows synergistic worsening of the mutant phenotypes, such as reduction of the telencephalon (arrows) and eye size, upon combined depletion of *gnl2* and *ns*. All images are lateral view, with anterior to the left and dorsal up. d, dorsal diencephalon; e, eye; h, hindbrain; hv, hindbrain ventricle; ot, optic tectum. Scalebar 125 μm.

retina from 30 hpf onwards (Figs. 2F and G). At 48 hpf, *gnl2* expression was restricted to the remaining proliferating zones of the brain, consisting of the posterior tectum, hindbrain and dorsal diencephalon (Fig. 2G), and to the ciliary marginal zone (CMZ) of the retina that retains proliferative activity in adult fish (Raymond et al., 2006; Wullimann and Knipp, 2000). In *gnl2* mutants, expression of *gnl2* was decreased at 30 hpf, suggesting nonsense-mediated decay of the mutant transcript (data not shown). High levels of *ns* mRNA expression was observed in regions of proliferative activity such as the optic tectum, retina and hindbrain, although in general *ns* expression was more restricted than that of *gnl2* (Figs. 2H and I). At 48 hpf, *ns* was expressed in the optic tectum, dorsal tel- and diencephalon, hindbrain and in the retinal CMZ (Fig. 2I). In *ns* mutants, *ns* transcripts were decreased at 30 hpf (data not shown), suggesting nonsense-mediated decay of the *ns* mutant transcript as well.

Although we do not know the expression profiles of Gnl2 and NS proteins in the zebrafish, the similar expression patterns of *gnl2* and *ns* mRNAs in combination with their similar morphological phenotypes suggest that Gnl2 and NS may function redundantly.

To investigate this, *gnl2*/*ns* compound heterozygous carriers were generated and the phenotypes of their progeny were examined. Prior to 36 hpf, compound *gnl2*/*ns* homozygous mutants did not appear significantly different from the *gnl2* mutant (data not shown). From 36 hpf onwards, double mutants were apparent by a synergistic phenotype resulting in a further reduction of eye size and a more severe hyperinflation of the hindbrain ventricle (Figs. 2J–M; Suppl. Figs. 2A and B). At 72 hpf, the body length, head size, and eye size of the compound mutants were dramatically reduced compared to the WT, *gnl2*, or *ns* single mutant siblings (Suppl. Figs. 2B and C). These synergistic phenotypes suggest that *gnl2* and *ns* indeed function at least in part redundantly. To further test redundancy of Gnl2 and NS, we investigated whether misexpression of WT *gnl2* or *ns* mRNA was able to improve the *ns* and *gnl2* mutant phenotypes, respectively. Indeed, injection of 475 pg of WT *gnl2* mRNA was able to partially restore head and eye size of *ns* mutants (Suppl. Fig. 2D). Conversely, injection of 500 pg of WT *ns* mRNA into *gnl2* mutants resulted in a similar partial rescue (Suppl. Fig. 2D), indicating that *gnl2* and *ns* are able to compensate at least partially for the loss of the other gene.

Loss of NS and/or Gnl2 causes delayed differentiation of retinal progenitors

The decrease of expression levels of *gnl2* and *ns* during development appears to be correlated with decreased proliferation rates as development proceeds. In addition, the domains that retain high levels of *gnl2* and *ns* expression represent regions that are known to maintain their proliferative capacity in postembryonic stages. These facts are highly suggestive of a function of *gnl2* and *ns* in maintaining populations of neural progenitors.

The zebrafish retina is easily accessible for analysis of cell fate acquisition as it consists of a highly ordered structure containing a limited number of neuronal cell types (Stenkamp, 2007). Thus, we elected to analyze retinal neurogenesis in *gnl2*, *ns*, and *gnl2*/*ns* double mutants to further investigate the effects of *gnl2* and *ns* depletion on proliferation and differentiation.

Histological sections reveal incomplete formation of the retinal ganglion cell layer (GCL) and inner and outer nuclear layers (INL, ONL) of the retina in *gnl2* and *ns* mutants at 72 hpf as compared to WT embryos (Figs. 3A–C). The total number of nuclei in the *gnl2* and *ns* mutants as compared to WTs was slightly reduced at 30 hpf (data not shown) and was about two-fold reduced at 48 hpf (554 ± 59 cells in WT retina ($n = 6$), 284 ± 18 cells in *gnl2* ($n = 3$) and 274 ± 52 cells in *ns* ($n = 3$; Student's *t*-test, $p < 0.01$). However, retinal development in general was not delayed, as pigment formation occurred normally and on time (data not shown).

We next investigated the differentiation of retinal neuronal and glial cell types in the *gnl2* and *ns* mutants. In WT zebrafish embryos prior to 28 hpf, all neural retina precursors are proliferating. Expression of the bHLH transcription factor *ath5* marks retinal progenitors preceding their final cell cycle exit and is first induced in the ventronasal retina (Kay et al., 2001, 2005). Subsequently, its expression progresses through the retina, preceding the wave of retinal ganglion cell (RGC) differentiation (Fig. 3D). In *gnl2* mutants (Fig. 3E), only a few cells expressing *ath5* were present in the retina at 36 hpf, contrasting in contrast with its broad expression in WT retinae (Fig. 3D). In contrast, *ath5* expression in *ns* mutants was relatively normal at 36 hpf (Fig. 3F). At 48 hpf, *ath5* expression was present throughout the prospective RGC layer in *gnl2* and *ns* mutants, similar to *ath5* expression in WTs (data not shown).

Immunolabeling with zn8, an antibody that labels mature RGCs (Figs. 3G and J), showed a delay in RGC differentiation at 48 hpf in *gnl2* (Fig. 3H) and *ns* mutants (Fig. 3I). At 72 hpf, the GCL in *gnl2* mutants remained poorly differentiated with RGCs being localized only in the central retina directly behind the lens (Fig. 3K). Unlike *gnl2* mutants, the GCL was regularly shaped in *ns* mutants at 72 hpf. However, similar to *gnl2*, the GCL failed to extend around the lens completely (Fig. 3L). In *gnl2*/*ns* compound mutants, differentiated RGCs were only present in a small portion of the central retina, showing a synergistic effect of the loss of Gnl2 and NS on RGC differentiation (Fig. 3V). The delay in RGC differentiation in *gnl2* and *ns* mutants was confirmed by delayed and reduced expression of *irx1a*, a marker for early differentiated RGCs (data not shown).

Differentiation of amacrine cells in the zebrafish inner nuclear layer (INL) starts around 35 hpf (Fig. 3M). Amacrine cells were reduced in *gnl2* (Fig. 3N) and *ns* mutants (Fig. 3O) at 48 hpf as observed using HuC/D labeling, which labels RGCs and amacrine cells. Photoreceptor cells start to differentiate in the zebrafish outer nuclear layer (ONL) around 43 hpf (Fig. 3P). In *gnl2* mutants, cone photoreceptor cells as labeled with zpr1 were present only in the central retina (Fig. 3Q). In *ns* mutants, cone photoreceptor cells were present almost throughout the ONL, indicating their normal differentiation (Fig. 3R). In *gnl2*/*ns* compound mutants, no cone photoreceptor cells were observed (Fig. 3W).

The last cell type in the zebrafish retina that initiates terminal differentiation around 48 hpf is the Müller glial cell, which has its soma located in the INL and its processes extending towards the basal and apical surfaces (Fig. 3S). Using the zrf1 antibody (α-GFAP) that labels Müller glial cells, we observed a marked reduction of Müller glial somata and their processes in *gnl2* mutants (Fig. 3T). In addition, there was an ectopic expression of zrf1 in the inner limiting membrane that separates the retina and vitreous body, which suggests a defect in the Müller endfeet that terminate here. When we examined the *gnl2* retina using an antibody to glutamine synthase, another marker of glial cells, we observed abnormal distribution of Müller glial somata in the INL of *gnl2* mutants (Suppl. Fig. 3). In addition, there were glial cells expressing high levels of glutamine synthase immediately surrounding the optic nerve, with their apical endfeet ending at the inner limiting membrane. These cells could be reactive astrocytes or premature reticular astrocytes that develop from optic stalk cells (Maggs and Scholes, 1990). In contrast to *gnl2*, Müller glial cells were present in the *ns* mutant GCL in a relatively normal pattern (Fig. 3U). In compound *gnl2*/*ns* mutants, Müller glial cells were almost entirely absent (Fig. 3X).

Taken together, these data show that the impaired RGC differentiation due to loss of *gnl2* or *ns* is not accompanied by adoption of alternate later retinal cell fates by the precursors. In addition, the data show that the timing of neuronal and glial differentiation is affected more severely in *gnl2* mutants than in *ns* mutants. The combined loss of *gnl2* and *ns* causes even more severe delays in differentiation up to a

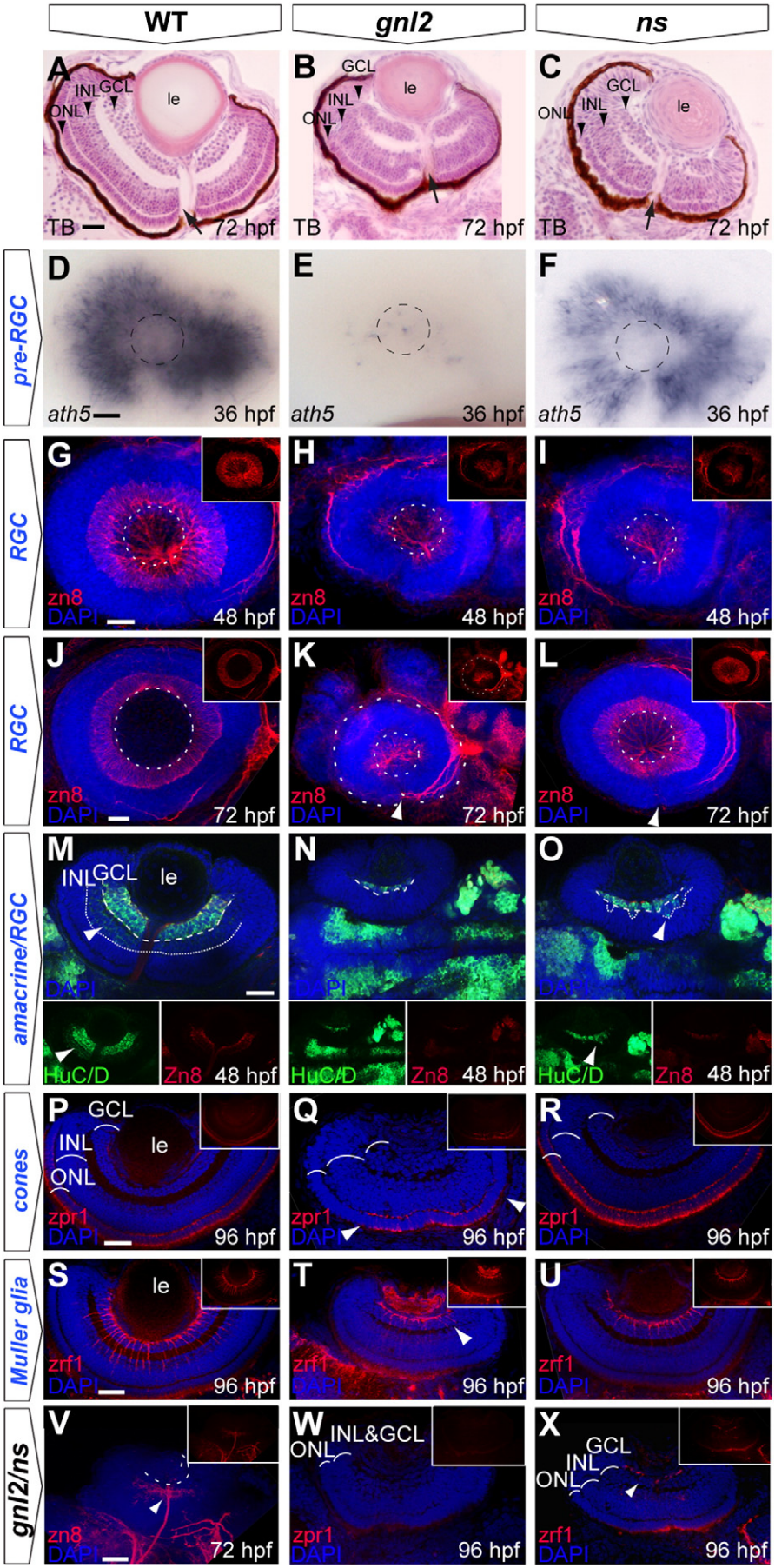
WT
gnl2
ns
A
B
C
GCL
INL
ONL
le
TB
72 hpf
pre-RGC
D
E
F
ath5
36 hpf
RGC
G
H
I
zn8
DAPI
48 hpf
RGC
J
K
L
72 hpf
amacrine/RGC
M
N
O
HuC/D
Zn8
48 hpf
cones
P
Q
R
zpr1
96 hpf
Muller glia
S
T
U
zrf1
gnl2/ns
V
W
X
INL&GCL

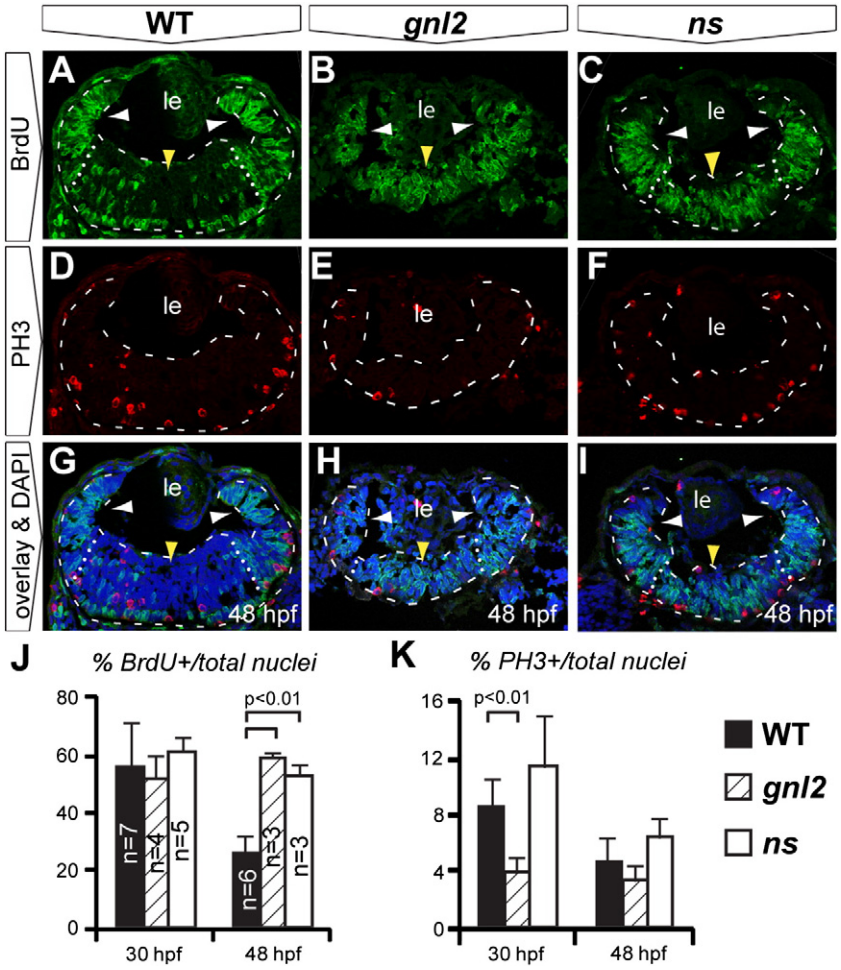

Fig. 4. Upon Gnl2 and NS loss of function, retinal progenitors fail to exit the cell cycle in a timely manner. (A–J). Confocal images of BrdU (green) and PH3 (red) double immunolabelling with DAPI overlay (blue) in WT (A, D and G), *gnl2* (B, E, H) and *ns* (C, F and I) embryos at 48 hpf. Retinae are outlined with dashed lines and subdivided into the peripheral (white arrowheads) and central retinae (yellow arrowhead) by dotted lines. In *gnl2* (B) and *ns* (C) embryos at 48 hpf, many BrdU+ cells are present throughout the central retina (yellow arrowheads), whereas in the WT, BrdU+ cells are mainly found at the retinal margin (white arrowheads). The number of PH3+ cells is slightly decreased in *gnl2* mutants (E), but not in *ns* mutants (F). (J) Quantification of the percentage of BrdU+ cells over the total cell number shows that there is no difference at 30 hpf. At 48 hpf, significantly more retinal cells are undergoing S-phase in *gnl2* and *ns* mutants. (K) Quantification of the percentage of PH3+ cells over total cell number shows a reduction in cells undergoing M-phase in *gnl2*, but not in *ns* mutants. Lateral is up, anterior to the left. Statistics: Student's *t*-test. p-values and experimental numbers indicated in graph. Error bars represent SD. Scalebar 25 μm.

point that the last retinal cell types to differentiate (photoreceptors and Müller glia) are absent or drastically reduced.

Loss of gnl2 and ns results in aberrant expression of cell cycle markers

Delayed terminal neuronal differentiation of retinal precursor cells may be due to the inability of precursors to exit the cell cycle. To determine the proportion of retinal cells in S- and M-phase, we analyzed BrdU-incorporation and cells expressing phosphorylated histone 3 (PH3), respectively, at 30 and 48 hpf (Fig. 4). At 30 hpf, many cells in the WT retina are proliferating as visualized by BrdU labeling (Fig. 4J). In *gnl2* and *ns* mutants, there was no difference at 30 hpf in the percentage of BrdU-positive cells/retina (Fig. 4J) as compared to WTs. However, the percentage of PH3-positive cells/total

Fig. 3. Delayed RGC differentiation in the *gnl2* and *ns* mutant retina. (A–C) Transverse toluidine-blue stained sections of WT (A), *gnl2* (B) and *ns* (C) showing incomplete formation of GCL, INL and ONL at 72 hpf (arrowheads). Arrow indicates optic nerve head. (D–F) Expression of *ath5* marks retinal progenitors prior to cell cycle exit. At 36 hpf, *ath5* is absent apart from a few cells in *gnl2* mutants (E; n = 7 embryos), whereas its expression is reduced, but is normally patterned in *ns* mutants (F; n = 6). Dashed circle indicates the outline of the lens. (G–L) Confocal images of immunolabelings to the RGC marker zn8 (red) with DAPI nuclear counterstaining (blue) at 48 (G–I) and 72 (J–L) hpf. In *gnl2* mutants, the GCL is disorganized and reduced in width at both 48 hpf (H; n = 11) and 72 hpf (K; n = 25). In *ns* mutants, formation of the GCL layer is incomplete at 48 hpf (I; n = 22), but has markedly improved at 72 hpf (L; n = 19). Insets show single zn8 fluorescence views. Dashed circles indicate the outline of the lens; the additional outer circle in (K) delineates the outline of the eye. (M–O) Single confocal planes of Hu/D (green) and zn8 (red) labeling with DAPI nuclear counterstaining (blue), which labels RGCs and differentiated amacrine cells, and RGCs only, respectively, in *gnl2* (N; n = 5) and *ns* mutants (O; n = 6) at 48 hpf. Arrowhead shows amacrine cells that are labeled with HuC/D, but not with zn8. Dashed line shows boundary of GCL, dotted line marks boundary of amacrine cells in the INL. Insets show single HuC/D and zn8 fluorescence views. (P–R) At 96 hpf, differentiated photoreceptor cells marked by zpr1 staining in red with DAPI nuclear counterstaining (blue) are present in the central *gnl2* mutant retina only (boundaries indicated with arrowheads in Q; n = 8). In *ns* mutants, photoreceptor cells have differentiated and are present throughout the outer nuclear layer (R; n = 5). Insets show single zpr1 fluorescence views. (S–U) At 96 hpf, Müller glial cells, marked by zrf1 staining in red with DAPI nuclear counterstaining (blue), have developed relatively normally in *ns* mutants (U; n = 11), but are disorganized and reduced in *gnl2* mutants (arrowhead in T; n = 9). Insets show single zrf1 fluorescence views. (V–X) Differentiation of retinal cell types, such as RGCs (n = 5; V; compare to J), photoreceptor cells (n = 4; W, compare to P) and Müller glial cells (n = 3; X, compare to S) is severely affected in *gnl2*/*ns* compound mutants as compared to WTs. Inset show single fluorescence view. (A–C) Lateral up, anterior to the left. (D–L) Lateral view, anterior to the left and dorsal up. (M–X) Dorsal view, with anterior to the left. GCL, ganglion cell layer; INL, inner nuclear layer; le, lens; ONL, outer nuclear layer. Scalebar 25 μm.

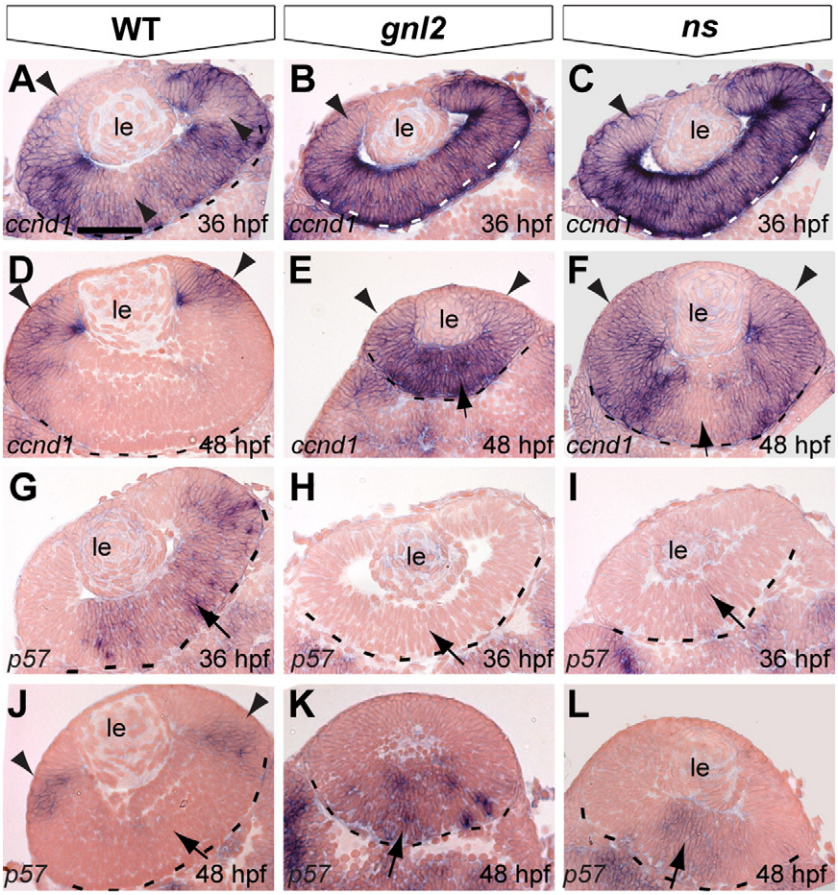

Fig. 5. Aberrant expression of cell cycle regulators in *gnl2* and ns mutant retinae. (A–F) Transverse sections showing expression of *ccnd1* at 36 hpf (A–C) and 48 hpf (D–F). In the WT retina, a subset of cells has downregulated *ccnd1* (arrowheads in A), indicating their withdrawal from the cell cycle. At 48 hpf, *ccnd1* is restricted to the ciliary marginal zone that remains proliferative (arrowheads in D). In contrast, *ccnd1* is not downregulated in *gnl2* (n = 10; B) or *ns* (n = 10; C) mutant retinae at 36 hpf (arrowheads) and remains expressed in the central retina of *gnl2* mutants (n = 9; arrow in E). In *ns* mutants, *ccnd1* expression is downregulated in the central retina (n = 9; arrow in F), but remains expressed in the remainder of the retina (arrowheads). (G–L) Sections showing expression of *p57kip2* in the WT central retina at 36 hpf (arrow in G). In contrast, there is no expression in *gnl2* (n = 11; H) and *ns* (n = 9; I) mutant retinae (arrows). At 48 hpf, *p57kip2* expression is restricted to the lateral surface of the retina in WTs (arrowheads in J). In contrast, *p57kip2* is expressed in the central retina of *gnl2*, (n = 12; arrow in K) and *ns* mutants (n = 13; arrows in L). Dashed lines indicate outline of the retina. Dorsal view, anterior to the left. le, lens. Scalebar 25 μm.

number of retinal cells was significantly reduced in *gnl2* mutants at 30 hpf (Fig. 4K). At 48 hpf, most cells in the central WT retina have exited the cell cycle as they no longer incorporate BrdU (Fig. 4A). In contrast, many cells in the central retina of *gnl2* and *ns* mutants are still BrdU-positive (Figs. 4B, C and J). Intriguingly, the percentages of PH3-positive cells in the whole retina of *gnl2* and *ns* mutants were not similarly increased (Figs. 4D–F and K). Thus, loss of Gnl2 and NS (to a lesser degree) causes a relative decrease in the number of cells in M-phase as opposed to the number of cells in S-phase (Fig. 4K).

The cell cycle regulator Cyclin D1 (Ccnd1) promotes proliferation, whereas p57Kip2 (also known as Cdkn1c) inhibits G1-S-phase transition by inhibiting PCNA-mediated DNA replication (Watanabe et al., 1998) as well as by inhibiting cyclinD–CDK4/6 complexes (Besson et al., 2008). In the zebrafish retina, forced expression of *p57kip2* induces cell cycle exit of retinal progenitors (Shkumatava and Neumann, 2005). In WT retinae, *ccnd1* expression is present throughout the retina at 36 hpf and progressively restricted during retinal neurogenesis to only the CMZ at 48 hpf (Figs. 5A and D). In *gnl2* and *ns* mutants, *ccnd1* failed to be timely downregulated and remained expressed in the central retina at 48 hpf (Figs. 5B, C, E and F), indicating that more retinal precursors in the mutants continued to cycle. Conversely, expression of the CDK inhibitor *p57kip2* was absent in the *gnl2* and *ns* retina at 36 hpf (Figs. 5H and I), whereas it was expressed in the central WT retina (Fig. 5G). At 48 hpf, *p57kip2* was

Fig. 6. p53 stabilization upon loss of Gnl2 and NS causes apoptosis and differentially affects retinal differentiation. (A) Western blot analysis of p53 (top panel) shows stabilization of p53 protein in *gnl2* and *ns* mutants at 48 hpf (left and middle panel) and *ns* mutants at 96 hpf (right panel) in comparison to low levels of p53 protein in WT embryos. As a control, stabilization of p53 upon exposure to 25 Gy of γ-irradiation is shown. Irradiation of *gnl2* and *ns* mutants does not visibly increase p53 levels. The loading control for actin is shown in the bottom panel. (B–G) Tunel assay showing presence of apoptotic cells in *gnl2* (C; n = 6) and *ns* mutants (D; n = 6) at 48 hpf with the highest incidence in the optic tectum. In *ns* mutants, apoptosis was less pronounced as compared to *gnl2* mutants. (E–G) Upon injection of 1 ng of p53 MO, apoptosis is dramatically reduced in *gnl2* (F; n = 13) and *ns* mutants (G; n = 16). Injection of p53 MO has no effect on cell survival in WT embryos (E; n = 57). (H–S) Confocal views of immunolabeling with zn8 antibody (green) that marks mature RGCs, with DAPI nuclear counterstaining (blue). (K–M) and (Q–S) show single zn8 fluorescence. Dashed lines indicate the outline of the lens. At 72 hpf, the GCL in WT (H and K) and single *p53* mutants (n = 4; N and Q) has extended around the lens in a cup-like shape (arrows in K and Q). In contrast, *gnl2* (n = 5; I and L) and *ns* (n = 5; J and M) mutants lack a fully formed GCL (arrows in L and M) and RGCs are present only in the central retina. In *gnl2*/*p53* compound mutants (n = 3; O and R), differentiated RGCs were present only in the central retina and failed to extend around the lens (arrows in R) similar to single *gnl2* mutants (arrows in L). The optic nerve size was equivalent between single *gnl2* and compound *gnl2*/*p53* mutants (arrowheads in L and R). Similarly, the GCL in *ns*/*p53* compound mutants (n = 5; P and S) fails to extend around the lens properly (arrows in S) and the diameter of the optic nerve is similar to that of single *ns* mutants (arrowheads in M and S). (B–J and N–P) Lateral view, anterior to the left, dorsal up. (K–M and Q–S) Dorsal view, anterior to the left. di, diencephalon; h, hindbrain; ot, optic tectum; t, telencephalon; uic, uninjected control. Scalebar (B–G) 125 μm, (H–P) 25 μm.

expressed only in the CMZ in WTs (Fig. 5J), whereas it was present in the central retina of *gnl2* and *ns* mutant (Figs. 5K and L), suggesting a delayed onset of *p57kip2* expression in mutant retinae.

The above data show that in the *gnl2* and *ns* mutant retina, precursors continue to express cell cycle regulators and show delayed expression of cell cycle exit markers. These defects may cause the observed delays in cell cycle exit and terminal neuronal differentiation. Surprisingly, the loss of Gnl2 causes premature neuronal differentiation in the developing brain (Figs. 1A–H). Similar to *gnl2*, the expression domain of the proneural gene a*scl1a* was expanded in

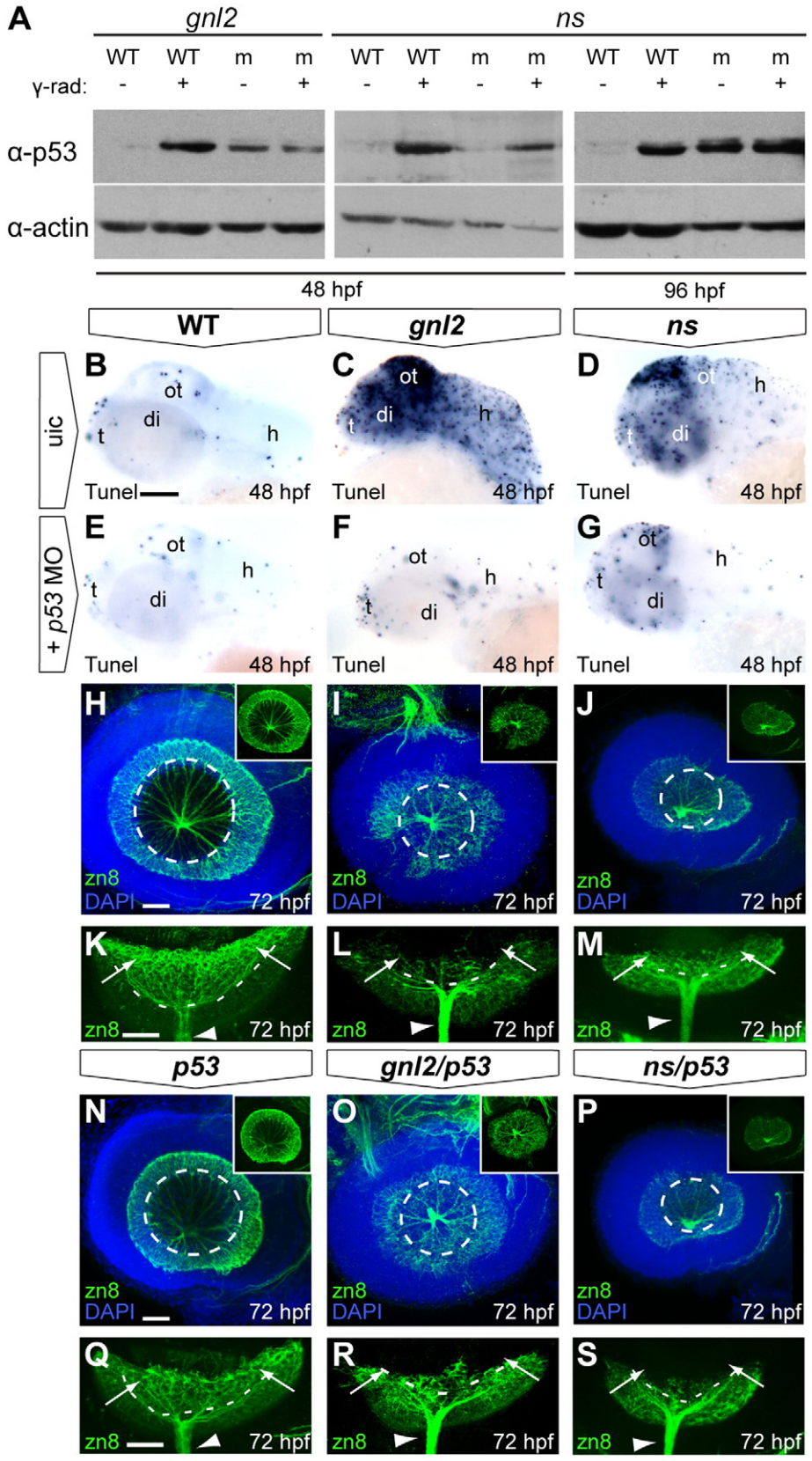

the *ns* mutant brain (data not shown). At 30 hpf, *ccnd1* expression was expanded in the *gnl2* and *ns* brain (Suppl. Figs. 4A–C). Intriguingly, the expression of *p57kip2* was also expanded in the *gnl2* and *ns* mutant brain from 30 hpf (Suppl. Figs. 4D–F). These data suggest that in the brain, premature cell cycle exit occurs in contrast to the retina where late cell cycle exit occurs (Figs. 5L–Q). At 48 hpf, *ccnd1* expression was increased predominantly in the dorsal midbrain (Suppl. Figs. 4G–L). At the same time, *p57kip2* expression in the brain was reduced in the *gnl2* fore- and dorsal midbrain as compared to WTs but relatively increased in ventral midbrain and diencephalon (Suppl. Figs. 4M–R). These data suggest that the different effects of Gnl2 and NS loss of function on neurogenesis in the brain and retina may be the consequence of differential expression of the cell cycle inhibitor *p57kip2*.

Gene expression changes upon loss of Gnl2

Because little is known about the function of Gnl2 in vertebrates, we examined the gene expression profile of *gnl2* mutant versus WT embryos using microarray analysis. The gene expression profile was examined at 22 hpf, which was the earliest development stage at which the *gnl2* mutant phenotype could be readily identified (Suppl. Figs. 5A and B). Statistical analysis revealed 96 significantly up- and 44 downregulated genes with an at least 1.5-fold change in expression and a p-value<0.05 (Suppl. Table 1). Of these genes, 64 up- and 26 downregulated genes had a known Gene Ontology (GO) biological process function (Suppl. Fig. 5C).

Functional characterization of the downregulated genes showed that about 30% of downregulated genes are regulators of transcription (*zbtb16*, *rdbp*, *vsx2*, *otp*, *pcid2*, *sox2*, *pias4*) or genes encoding proteins involved in ribosome biogenesis (*rpl22l1*, *rps16*, *rpl30*, *gnl2*). Furthermore, several pro-apoptotic and apoptosis-mediating genes (*dedd1*, *dap1b*, *gadd45gl*, *dnase1l3*) were downregulated. In the upregulated group of genes, many components of the p53-cell death pathway were present (*p53*, *bnip3*, *bax*, *vrk2*, *gadd45al*, *sesn3*, *casp8*, *ccng1*). Other upregulated genes involved in cell cycle arrest were *h2afx* and *cdkn1bl*. Importantly, expression of *mdm2*, which is a direct target of p53, was found to be upregulated. There was no change in expression levels of *ccnd1* or *p57kip2* at this stage.

To confirm the microarray results, *in situ* hybridizations were performed for *gnl2* and two direct transcriptional targets of p53, *mdm2* (Wu and Levine, 1997) and *ccng1* (Okamoto and Beach, 1994). In agreement with the microarray data, *in situ* hybridizations showed reduction of *gnl2* (Suppl. Figs. 5D and E) and induction of both *mdm2* (Suppl. Figs. 5F and G) and *ccng1* expression (Suppl. Figs. 5H and I) in the *gnl2* mutant brain at 22 hpf. Expression of these genes was indistinguishable between WT and *gnl2*$^{+/-}$ embryos (data not shown).

p53 activation causes apoptosis in gnl2 and ns mutants

The *gnl2* expression profile suggests that Gnl2 loss of function causes p53 stabilization and activation. NS loss of function has previously been shown to cause p53 activation *in vitro* (Ma and Pederson, 2007; Meng et al., 2008; Tsai and McKay, 2002). We evaluated p53 stabilization in *gnl2* and *ns* mutants by Western blotting using a zebrafish-specific monoclonal p53 antibody (MacInnes et al., 2008). In *gnl2* and *ns* mutant embryos at 48 hpf and 96 hpf, respectively, p53 protein is found to be stabilized in the absence of γ-irradiation, with no apparent increase in stabilization observed upon the application of γ-irradiation (Fig. 6A). However, we detected very little stabilization of p53 in the *ns* mutants at 48 hpf (Fig. 6A). This suggests that the loss of both Gnl2 and NS in zebrafish embryos induces the stabilization of p53 and that the results are consistent with the observation that the *gnl2* mutant phenotype is more severe than that of *ns*.

Since p53 activation can induce programmed cell death, we examined the number of apoptotic cells in *gnl2* and *ns* mutants using TUNEL analysis. Indeed, more apoptotic cells were observed throughout the brain of *gnl2* and *ns* mutants at 30 hpf as compared to WTs (data not shown). At 48 hpf, many apoptotic cells were present throughout the *gnl2* brain (Fig. 6C) and to a lesser extent in the *ns* brain (Fig. 6D). To evaluate the contribution of p53 activation to the *gnl2* and *ns* apoptosis phenotypes, a p53 translation-blocking morpholino was injected and apoptotic cells were evaluated at 30 (data not shown) and 48 hpf (Figs. 6E–G) by Tunel assay and Acridine Orange labeling of apoptotic cells (data not shown). Injection of 1 ng p53 MO, a concentration previously shown to rescue apoptosis induced by Mdm2 knockdown in zebrafish (Langheinrich et al., 2002), dramatically reduced apoptosis throughout the brain and retinas in both mutants as visualized by Tunel (Figs. 6F and G). The contribution of activated p53 to the apoptotic phenotype is reflected by the ameliorated morphology of the *gnl2* and *ns* mutant brains (data not shown). However, the eye and head size of the MO-injected mutants remained noticeably smaller in comparison to their WT siblings and the lethality of the embryos remained the same as their non-injected mutant cohorts.

p53 activation does not cause the delayed neuronal differentiation in the gnl2 and ns retina

As knockdown of p53 does not appear to rescue the *gnl2* and *ns* mutants' lethal phenotype fully, we next investigated the p53-dependence of the mutants' differentiation phenotypes and analyzed RGC differentiation in *gnl2* and *ns* mutants upon additional depletion of p53. p53 was ablated either by injection of p53 MO or by crossing *gnl2* or *ns* mutants into a previously described zebrafish *tp53*$^{M214K/M214K}$ mutant loss of function line (Berghmans et al., 2005).

The *ath5* and *irx1a* expression domains that indicate proneural and early RGC fate, respectively, were absent in single *gnl2* (n=8) and compound *gnl2/p53* mutants (n=3) at 36 hpf (Figs. 3D and E and data not shown). At 48 hpf, the *irx1a* expression domain did not completely surround the lens in single *gnl2* (n=6) and *gnl2/p53* compound mutants (n=3; data not shown). Immunolabeling of embryos with zn8 showed that differentiated RGCs were present only in the central retina of *gnl2* and *gnl2/p53* compound mutants at 48 (data not shown; n=4) and 72 hpf (Figs. 6I, L, O and R), suggesting that p53 reduction did not prevent the delay in RGC differentiation caused by Gnl2 loss of function. Similar results were obtained by injection of p53 MO into *gnl2* mutants (Suppl. Figs. 6B, E and G). In

Fig. 7. Gnl2 acts non-cell autonomously in retinal cell cycle exit and differentiation. (A) Experimental setup. Cells are taken from sphere-stage donor embryos that have been injected with fluorescein-dextran and biotin-dextran and are subsequently transplanted into the prospective eye field of shield-stage unlabelled host embryos. Embryos were exposed to a 30-minute EdU pulse at 48 hpf and were fixed immediately. Clones were examined for the proportion of EdU+ proliferating cells and zn8+ RGCs. (B–E) Single-plane confocal images of clones of transplanted cells showing DAPI-counterstained nuclei (cyan, top left), streptavidin-Alexa488 (green, top right), EdU (white, bottom left) and zn8-stained RGCs (magenta, bottom right). Clones of transplanted cells are outlined by dotted lines (white or green). The retina is outlined with dashed white lines. Shown are clones transplanted from WT donor to WT host (B), WT donor to *gnl2* mutant host (C), 2 ng *gnl2* MO-injected donor to WT host (D) and 2 ng *gnl2* MO-injected donor to 2 ng *gnl2* MO-injected host (E). (F) Quantification of the percentage of EdU+ (black bars) and zn8+ RGCs (striped bars) within transplanted clones for each of the experimental groups. Statistics: Two-tailed Student's *t*-test, p-values indicated above the bars (*p<0.01, **p<0.02). Error bars represent the standard deviation. (G) Distribution of EdU+ cells within the clones of transplanted cells. The clones were divided along their baso-apical axis in 6 equidistant bins and the percentage of EdU+ cells/bin was determined. Clones from WT→WT and WT→*gnl2* mutant, and *gnl2*→WT and *gnl2*→*gnl2* show similar distribution of EdU+ cells along the apico-basal axis. In contrast, the distribution at bins 2 and 6 is significantly different between WT→WT and WT→*gnl2* mutant, and *gnl2*→WT and *gnl2*→*gnl2* clones. Statistics: Two-tailed Student's *t*-test. Error bars represent SEM. Scalebar 25 μm.

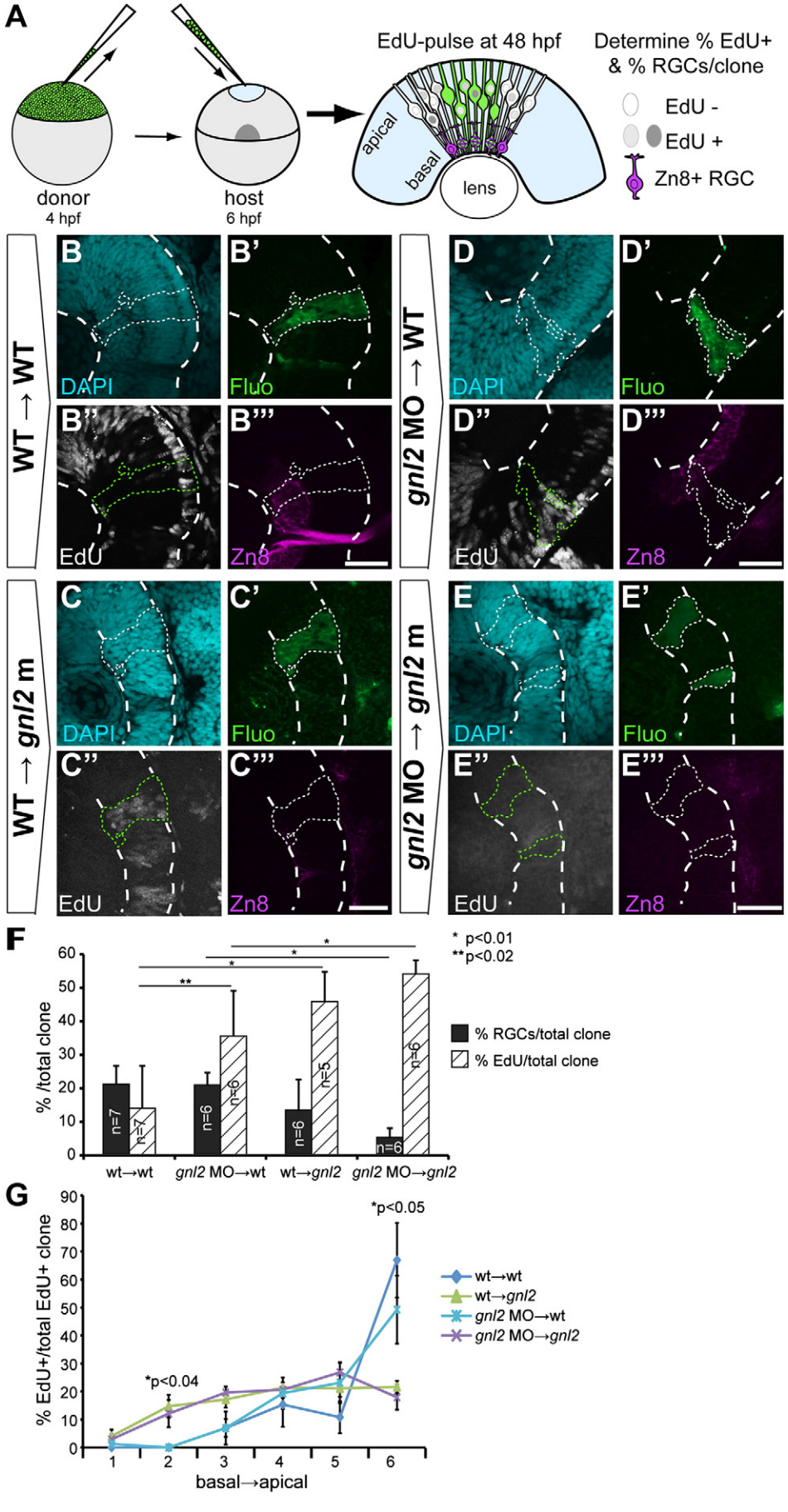
A
donor
4 hpf
host
6 hpf
EdU-pulse at 48 hpf
Determine % EdU+
& % RGCs/clone
EdU -
EdU +
Zn8+ RGC
apical
basal
lens
WT → WT
gnl2 MO → WT
WT → gnl2 m
gnl2 MO → gnl2 m
DAPI
Fluo
EdU
Zn8
F
* p<0.01
** p<0.02
% /total clone
% RGCs/total clone
% EdU/total clone
wt→wt
gnl2 MO→wt
wt→gnl2
gnl2 MO→gnl2
G
*p<0.05
*p<0.04
% EdU+/total EdU+ clone
basal→apical

addition, p53 MO injection did not increase the total number of nuclei in the *gnl2* retina (Suppl. Fig. 6H). These data suggest that although p53 stabilization is widely known to cause cell cycle arrest, this arrest is not responsible for the delayed differentiation of the *gnl2* mutant retinal cells. In contrast, injection of p53 MO into *ns* mutants increased the number of RGCs in *ns* mutants and partially rescued the number of retinal cells at 48 hpf (Suppl. Figs. 6C, F, I and J). However, the patterning of the GCL was not rescued as the GCL had not extended properly around the lens in *ns/p53* compound mutants at 72 hpf (Figs. 6J, M, P and S). These data suggest that the delayed neuronal differentiation phenotype in *gnl2* and *ns* mutants occurs mainly independently of p53 activation.

Gnl2 and NS have both non-autonomous and cell-autonomous functions in retinal progenitor cell cycle exit and differentiation

Since the delayed cell cycle exit and neuronal differentiation in *gnl2* and *ns* mutants occur independently of p53 activation, we next examined whether Gnl2 and NS act cell-autonomously or non-cell autonomously in retina progenitors by mosaic analysis. Cells from labeled sphere-stage embryos were transplanted into the prospective eye fields of unlabelled shield-stage host embryos (Fig. 7A). At 48 hpf, the transplanted host embryos were exposed to a short pulse of EdU to determine the proportion of cells in S-phase. Subsequently, transplanted embryos were examined for the EdU incorporation and the expression of the RGC marker zn8 (Suppl. Table 2).

As expected, most of the cells derived from WT donors that were transplanted in WT host retinae had exited the cell cycle by 48 hpf and ±20% of cells had differentiated into RGCs (Figs. 7B and F).

Intriguingly, when WT cells were transplanted into *gnl2* or *ns* mutant retinae, the proportion of EdU+ cells in WT clones was increased as compared to WT clones in a WT environment (Figs. 7C and F; Suppl. Figs. 7A–D). In addition, the proportion of differentiated RGCs in WT to *gnl2* or WT to *ns* transplantations was reduced. In very large clones (>300 cells), in a subset of cases, RGCs seemed to be induced in the middle of the clone (Suppl. Figs. 7F and G). However, more EdU+ cells were present in these clones than in large clones of WT cells in WT environments. These data suggest that Gnl2 and NS act non-cell autonomously.

In all transplantation experiments (for each mutant >200 host embryos transplanted with cells derived from the progeny of heterozygous parents), there were exceptionally few host embryos with healthy-looking transplanted cells derived from *gnl2* or *ns* mutant hosts. Also, in the embryos that did contain living mutant transplanted cells, in the majority of embryos, these living cells were present in the brain, but seldom in the retina. The only embryo containing living transplanted *gnl2* donor cells in a WT retina contained only a very small clone (12 cells). In this embryo, the mutant cells were able to differentiate into RGCs and only few cells were proliferating (Suppl. Fig. 7E). These data suggest that *gnl2* and *ns* mutant cells are very sensitive to induction of cell death upon transplantation, especially when targeted to a WT retina environment. To circumvent this, we used *gnl2* MO injection to evaluate the behavior of *gnl2*-reduced cells in WT and *gnl2* mutant environments. Embryos injected with 2 or 5 ng of *gnl2* MO showed a mild to severe *gnl2* mutant-like phenotype, respectively, with regards to EdU incorporation and RGC differentiation (data not shown). Transplantation of WT cells into host embryos that had been injected with 5 ng of *gnl2* MO showed reduced cell cycle exit and RGC differentiation (Suppl. Figs. 7E and H), confirming the results of the transplantation of WT into *gnl2* mutant environments. The proportion of EdU+ and zn8+ cells in WT clones in 5 ng *gnl2* MO environment was very similar to that of 5 ng *gnl2* MO clones in 5 ng *gnl2* MO environment (Suppl. Figs. 7E and I). Unfortunately, no WT host retinae (>150 total transplanted WT hosts) were observed to contain cells derived from 5 ng *gnl2* MO-injected donors, suggesting that similar to *gnl2* mutant cells, the morphant cells also died upon transplantation into WT retinae.

When cells derived from donors injected with 2 ng *gnl2* MO were transplanted, there were a small number of WT embryos containing small clones of living transplanted cells in the retina (Figs. 7D and F). In these embryos, the transplanted morphant cells showed a significantly reduced proportion of EdU+ cells and increased numbers of differentiated RGCs as compared to clones from 2 ng *gnl2* MO-injected donors in *gnl2* mutant retinae (Figs. 7E and F), suggesting that these morphant cells show increased cell cycle exit and RGC differentiation when placed in WT, but not mutant environments. Although the proportion of EdU+ cells in clones of *gnl2* morphant cells in WT retinae was decreased as compared to cells in mutant retinae, the proportion of EdU+ cells was still significantly higher ($p<0.02$) as compared to transplanted WT cells (Fig. 7F), suggesting that in this context Gnl2 also has some cell-autonomous function in cell cycle exit.

Next to the proportion of EdU+ cells within the clones, the distribution of EdU+ cells along the apico-basal axis within the clones was very similar between WT clones into WT host and *gnl2* MO into WT on the one hand and WT into *gnl2* and *gnl2* MO into *gnl2* host embryos on the other hand (Fig. 7G). These data confirm the non-cell autonomous function of Gnl2 in cell cycle exit and RGC differentiation.

Since the EdU detection method as used for the mosaic analysis experiments does not require denaturation and subsequent antibody detection (as with BrdU), but rather is a simple chemical 'click' reaction, this probably allows for determining quantitative differences in EdU incorporation representing differences in DNA synthesis between samples (Mahler et al., 2010; Salic and Mitchison, 2008). Indeed, when comparing the EdU label intensity between WT and *gnl2* or *ns* mutant retinae, considerable differences in EdU label intensity were observed that were not observed in the experiments using BrdU. In WT cells, two distinct EdU label patterns could be observed that represent the distinct phase of S-phase during the EdU exposure (Fig. 7B, Suppl. Fig. 7A). Some WT cells showed a punctate pattern of EdU incorporation, suggesting that these cells were only incorporating EdU for a limited time within the duration of the EdU pulse, probably at the very beginning or very end of the DNA synthesis stage. Other cells showed a more evenly distributed EdU label, suggesting that these cells were incorporating EdU for the whole duration of the EdU pulse. In contrast, the EdU label intensity was generally much lower in mutant cells and seemed to be more evenly distributed over the nuclei (especially in *gnl2* mutants; Fig. 7E, Suppl. Fig. 7B). This might reflect slower EdU incorporation due to slower DNA synthesis rates. Interestingly, the intensity difference remained noticeable in the transplantation experiments. The EdU intensity of transplanted WT cells in *gnl2* or *ns* mutant retinae was clearly much higher compared to surrounding mutant cells for all WT clones in all mutant embryos examined (Fig. 7C, Suppl. Fig. 7B and 8), suggesting that the effect of *gnl2* or *ns* depletion on EdU incorporation is cell-autonomous. Even in very large clones (>300 cells), this difference was apparent (Suppl. Figs. 7F and G). Interestingly, in the 2 ng *gnl2* MO clones in WT retinae, there was no apparent difference in EdU intensity between transplanted and directly surrounding cells (Suppl. Fig. 8F). Since we could not examine the EdU intensity of mutant cells in a WT environment, the cell-autonomous nature of the EdU intensity phenotype cannot be concluded with certainty.

Discussion

Nucleostemin has recently received a great deal of attention in the field of stem cells and cancer biology due to its role in maintenance of proliferation and its high expression in actively proliferating cells. However, the functions of the related protein Gnl2 have not been characterized in detail.

We demonstrate that the depletion of either Gnl2 or NS in the retina results in the failure of cells to exit the cell cycle and subsequent delayed terminal differentiation. In contrast, premature cell cycle exit and neuronal differentiation takes place in the brain. These defects appear to be linked to the aberrant expression of specific cell cycle regulators and not to cell cycle arrest caused by the stabilization of p53.

Partial redundancy between Gnl2 and NS was suggested by the synergistic worsening of the retinal differentiation phenotype in compound *gnl2*/*ns* mutants as compared to the respective single mutants. In general, the *gnl2* phenotype regarding p53 stabilization and retinal differentiation is more severe compared to the *ns* mutant phenotype. This difference could be due to differential expression of the two genes. This possibility is supported by the observation that *ns* expression is more restricted than that of *gnl2* during early development (<48 hpf). Alternatively, the difference in phenotype severity may reflect a differential contribution of maternal *gnl2* versus *ns* mRNA. Although further studies will be required to elucidate the extent of the overlapping functions of NS and Gnl2, our results do suggest that Gnl2 may in fact be more important than NS during development of vertebrate embryos.

Loss of Gnl2 and NS results in p53 stabilization and p53-mediated apoptosis

NS has recently been suggested to control p53 activity by binding to the E3 ubiquitin ligase Mdm2 or by increasing ribosomal protein L5 and L11 binding to Mdm2 (Dai et al., 2008). We demonstrate that depletion of NS and Gnl2 in the developing zebrafish causes stabilization of p53 and activation of p53 target genes. It has not been investigated whether Gnl2 can directly interact with Mdm2 similarly to NS. Our results show that depletion of Gnl2 causes stabilization of p53 protein as well as upregulation of the p53 target genes *ccng1* and *mdm2*, suggesting that such an interaction may exist.

Since survival of $Ns^{-/-}$ mice was not restored upon crossing the mutants with *p53* null mice, it was suggested that the relevance of p53-related functions of NS *in vivo* is small (Beekman et al., 2006). We show here that the induction of programmed cell death in *gnl2* and *ns* embryos is p53-dependent. This finding was corroborated by the upregulation of several pro-apoptotic genes that are induced by p53 activity in the *gnl2* expression profile. However, similar to the murine double *Ns*/*p53* mutants, we were unable to rescue the lethal phenotype of either the *gnl2* or *ns* mutant embryos by p53 depletion or by crossing the mutants with a loss of function p53 line. Moreover, we show here that p53 reduction does not restore the timing of RGC differentiation or survival of RGCs in *gnl2* mutants and thus, that p53 activation does not play a role in the neural differentiation defects. The RGC differentiation phenotype seemed initially improved upon depletion of p53 in *ns* mutants. Possibly, the reduction in differentiated neural cell types in the *ns* mutant retina is partially caused by increased apoptosis due to p53 activation.

Previous studies have shown that p53 activation and subsequent induction of apoptosis is common when ribosome biogenesis and translation are disrupted (Azuma et al., 2006; Chakraborty et al., 2009; Danilova et al., 2010; Skarie and Link, 2008; Zhang et al., 2003, 2008). Our and previous results show, however, that the direct contribution of p53 activation to the reduced health of the mutant retina appears to be small. Therefore, it seems probable that there must be pathways other than p53 that contribute to reduced health after cellular stresses such as reduced translation.

Gnl2 and NS are important for inducing timely cell cycle exit of neural progenitors

We show that mutations in *gnl2* or *ns* cause both delayed cell cycle exit and neuronal differentiation of retinal precursors. In *gnl2* mutants, induction of RGC fate was delayed. In contrast, RGC fate induction occurred normally in *ns* mutants. Previous studies have suggested that expression of Ath5 or p57Kip2 by itself is not sufficient to induce RGC fate, suggesting that combined expression of proneural genes with cell cycle inhibitors is required to promote neuronal differentiation (Ohnuma et al., 2002; Shkumatava and Neumann, 2005). Therefore, the prolonged expression of a cell cycle activator (*ccnd1*) in combination with prolonged incorporation of the S-phase marker BrdU and delayed expression of a cell cycle inhibitor (*cdkn1c*/*p57kip2*) in *gnl2* and *ns* mutant retinae suggests that the delayed differentiation is due to retinal precursors failing to exit the cell cycle on time.

The mosaic analysis experiments show that disruption of *gnl2* and *ns* result in both autonomous and non-cell autonomous defects in retinal development.

The non-cell autonomous aspects of the phenotype might reflect the general impaired health of the retina due to disruption of ribosome biogenesis that is known to result from loss of *gnl2* or *ns* (Bassler et al., 2001; Kudron and Reinke, 2008; Rosby et al., 2009; Saveanu et al., 2001). Reduced translation has also been previously shown to lead to delayed neurogenesis during development (Azuma et al., 2006). Therefore, it is very likely that defective translation could affect neuronal differentiation, perhaps by altering the status of signaling pathway(s) known to regulate steps in neurogenesis.

Intriguingly, several aspects of the *gnl2* and *ns* phenotypes appear to be cell-autonomous, namely the very low survival of *gnl2* and *ns*-donor derived transplanted cells in WT environments and the difference in EdU intensity. Also, it appears that Gnl2 and NS have a specific cell-autonomous function in the regulation of cell cycle exit in retinal progenitors. It is plausible that the Gnl2 and NS reduced cells have diminished health due to disrupted ribosome biogenesis and therefore, have reduced viability in comparison to surrounding healthy WT cells. The increased EdU-intensity of WT versus mutant cells that was conserved upon transplantation of WT cells into mutant environments and the increased proportion of EdU+ cells in morphant cells transplanted in WT environments as compared to transplanted WT cells suggests that there is a cell-autonomous function of Gnl2 and NS in S-phase progression.

The abnormally high expression levels of *ccnd1* in the *gnl2* and *ns* mutant retinae coupled to the increase in BrdU incorporation in the central retinae of the mutants provides strong evidence that cells in the mutant retinae are remaining in the cell cycle for a longer than normal length of time. In *gnl2* and to a lesser extent in *ns* mutants the number of cells undergoing mitosis relative to the number of cells in S-phase is decreased. This could mean that there is a delay or block in G2-M phase progression. However, we did not observe a significant difference in the proportion of Ph3+/BrdU+ cells in *gnl2* versus WT embryos in a 6 h BrdU chase-experiment (data not shown), suggesting that the G2-M phase progression is not affected. Alternately, an increase in total cell cycle length could be due to a shortening of M-phase or an increase in G1- or S-phase length. However, our results indicate that the most likely cell cycle alteration is the extension of S-phase length. The lower Edu intensity in *gnl2* mutants versus WT embryos could reflect a slower rate of DNA-synthesis in the mutants, possibly by activation of the intra-S-phase checkpoint for DNA repair. Therefore, more detailed analysis of the cell cycle and its regulators, in particular of S-phase entry and progression, could elucidate the exact role of Gnl2 and NS in regulation of cell cycle progression and exit. Also, it will be interesting to study in more detail whether and how Gnl2 and NS affect regulation of expression of cell cycle regulators such as Ccnd1 and p57kip2 directly.

An interesting aspect of the *gnl2* and *ns* mutants is the apparently contradicting phenotype in the brain versus retina. In contrast to the delayed cell cycle exit and decreased neuronal differentiation in the retina, premature neuronal differentiation was observed in the *gnl2* and *ns* brain (Fig. 1 and data not shown). A possible explanation is

given by the observation that *p57kip2* expression that is delayed in the retina is actually premature in the brain. Since *p57kip2* expression can drive cell cycle exit and induce neuronal differentiation (Park et al., 2005; Rothschild et al., 2006; Shkumatava and Neumann, 2005; Tury et al., 2011), it is plausible that this might drive the premature neuronal differentiation in the mutant brain. At this moment, we do not know what causes this difference in regulation of *p57kip2* expression levels. Another interesting observation regarding the difference in brain versus retinal phenotype is that the survival of mutant cells that were transplanted into the WT brain did not seem to be impaired to the same extent to that of mutant cells transplanted into the WT brain (data not shown). It will be interesting to study these differences between the brain and retina phenotypes further.

In summary, we demonstrate in this study that loss of either Gnl2 or NS in the developing vertebrate results in aberrant expression of cell cycle regulators, accompanied by delayed cell cycle exit and differentiation. The function of Gnl2 and NS in cell cycle exit and differentiation has both non-cell autonomous and cell-autonomous aspects and is independent of p53 stabilization. Moreover, unperturbed function of the nucleolar GTP-binding protein Gnl2 appears to be equally if not more important than that of NS for proper vertebrate development. Further studies evaluating the distinct and overlapping functions of Gnl2 and NS will be required to fully appreciate the roles of each protein in the regulation of proliferation of stem and cancer cells, as well as their roles in regulation of proliferation and differentiation during vertebrate development.

Role of the funding source

JP was supported by Netherlands Organisation for Scientific Research NWO Genomics grant #050-10-024 to the Zivkovic lab. AWM was funded by De Koninklijke Nederlandse Akademie van Wetenschappen (KNAW). These funding sources had no role in any part of this study or the preparation of this manuscript.

Supplementary materials related to this article can be found online at doi:10.1016/j.ydbio.2011.04.028.

Acknowledgments

The authors wish to thank R. Boonen, A. Brouwers and S. van de Water for technical assistance, F. van Eeden and V. Guryev for advise on positional cloning, J. Korving for histological sectioning, F. Bos and J. Kaslin for the kind gift of p53 morpholino and GS antibody, and L. van der Flier and B. Hogan for advise on the microarray experiment. We acknowledge the Hubrecht TILLING team for the ns mutant. We thank Prof. W. Huttner for facilitating use of the Olympus FV1000 microscope. We thank Prof. J. den Hertog and Prof. S. Schulte-Merker for critical reading of the manuscript, and Dr. Rene Ketting for helpful discussions. The Hubrecht Institute Animal Care Facility is thanked for services rendered.

References

Allende, M.L., Weinberg, E.S., 1994. The expression pattern of two zebrafish achaete-scute homolog (ash) genes is altered in the embryonic brain of the cyclops mutant. Dev. Biol. 166, 509–530.

Amsterdam, A., Burgess, S., Golling, G., Chen, W., Sun, Z., Townsend, K., Farrington, S., Haldi, M., Hopkins, N., 1999. A large-scale insertional mutagenesis screen in zebrafish. Genes Dev. 13, 2713–2724.

Azuma, M., Toyama, R., Laver, E., Dawid, I.B., 2006. Perturbation of rRNA synthesis in the bap28 mutation leads to apoptosis mediated by p53 in the zebrafish central nervous system. J. Biol. Chem. 281, 13309–13316.

Bassler, J., Grandi, P., Gadal, O., Lessmann, T., Petfalski, E., Tollervey, D., Lechner, J., Hurt, E., 2001. Identification of a 60S preribosomal particle that is closely linked to nuclear export. Mol. Cell 8, 517–529.

Beekman, C., Nichane, M., De Clercq, S., Maetens, M., Floss, T., Wurst, W., Bellefroid, E., Marine, J.C., 2006. Evolutionarily conserved role of nucleostemin: controlling proliferation of stem/progenitor cells during early vertebrate development. Mol. Cell. Biol. 26, 9291–9301.

Berghmans, S., Murphey, R.D., Wienholds, E., Neuberg, D., Kutok, J.L., Fletcher, C.D., Morris, J.P., Liu, T.X., Schulte-Merker, S., Kanki, J.P., Plasterk, R., Zon, L.I., Look, A.T., 2005. tp53 mutant zebrafish develop malignant peripheral nerve sheath tumors. Proc. Natl. Acad. Sci. U. S. A. 102, 407–412.

Besson, A., Dowdy, S.F., Roberts, J.M., 2008. CDK inhibitors: cell cycle regulators and beyond. Dev. Cell 14, 159–169.

Chakraborty, A., Uechi, T., Higa, S., Torihara, H., Kenmochi, N., 2009. Loss of ribosomal protein L11 affects zebrafish embryonic development through a p53-dependent apoptotic response. PLoS One 4, e4152.

Cheng, C.W., Hui, C., Strahle, U., Cheng, S.H., 2001. Identification and expression of zebrafish Iroquois homeobox gene irx1. Dev. Genes Evol. 211, 442–444.

Dai, M.S., Sun, X.X., Lu, H., 2008. Aberrant expression of nucleostemin activates p53 and induces cell cycle arrest via inhibition of MDM2. Mol. Cell. Biol. 28, 4365–4376.

Danilova, N., Kumagai, A., Lin, J., 2010. p53 upregulation is a frequent response to deficiency of cell-essential genes. PLoS One 5, e15938.

Diks, S.H., Bink, R.J., van de Water, S., Joore, J., van Rooijen, C., Verbeek, F.J., den Hertog, J., Peppelenbosch, M.P., Zivkovic, D., 2006. The novel gene asb11: a regulator of the size of the neural progenitor compartment. J. Cell Biol. 174, 581–592.

Guryev, V., Koudijs, M.J., Berezikov, E., Johnson, S.L., Plasterk, R.H., van Eeden, F.J., Cuppen, E., 2006. Genetic variation in the zebrafish. Genome Res. 16, 491–497.

Harada, T., Harada, C., Parada, L.F., 2007. Molecular regulation of visual system development: more than meets the eye. Genes Dev. 21, 367–378.

Horn, H.F., Vousden, K.H., 2007. Coping with stress: multiple ways to activate p53. Oncogene 26, 1306–1316.

Kay, J.N., Finger-Baier, K.C., Roeser, T., Staub, W., Baier, H., 2001. Retinal ganglion cell genesis requires lakritz, a Zebrafish atonal Homolog. Neuron 30, 725–736.

Kay, J.N., Link, B.A., Baier, H., 2005. Staggered cell-intrinsic timing of ath5 expression underlies the wave of ganglion cell neurogenesis in the zebrafish retina. Development 132, 2573–2585.

Kudron, M.M., Reinke, V., 2008. *C. elegans* nucleostemin is required for larval growth and germline stem cell division. PLoS Genet. 4, e1000181.

Langheinrich, U., Hennen, E., Stott, G., Vacun, G., 2002. Zebrafish as a model organism for the identification and characterization of drugs and genes affecting p53 signaling. Curr. Biol. 12, 2023–2028.

Ma, H., Pederson, T., 2007. Depletion of the nucleolar protein nucleostemin causes G1 cell cycle arrest via the p53 pathway. Mol. Biol. Cell 18, 2630–2635.

Ma, H., Pederson, T., 2008. Nucleostemin: a multiplex regulator of cell-cycle progression. Trends Cell Biol. 18, 575–579.

MacInnes, A.W., Amsterdam, A., Whittaker, C.A., Hopkins, N., Lees, J.A., 2008. Loss of p53 synthesis in zebrafish tumors with ribosomal protein gene mutations. Proc. Natl. Acad. Sci. U. S. A. 105, 10408–10413.

Maggs, A., Scholes, J., 1990. Reticular astrocytes in the fish optic nerve: macroglia with epithelial characteristics form an axially repeated lacework pattern, to which nodes of Ranvier are apposed. J. Neurosci. 10, 1600–1614.

Mahler, J., Filippi, A., Driever, W., 2010. DeltaA/DeltaD regulate multiple and temporally distinct phases of notch signaling during dopaminergic neurogenesis in zebrafish. J. Neurosci. 30, 16621–16635.

Masai, I., Stemple, D.L., Okamoto, H., Wilson, S.W., 2000. Midline signals regulate retinal neurogenesis in zebrafish. Neuron 27, 251–263.

Meng, L., Zhu, Q., Tsai, R.Y., 2007. Nucleolar trafficking of nucleostemin family proteins: common versus protein-specific mechanisms. Mol. Cell. Biol. 27, 8670–8682.

Meng, L., Lin, T., Tsai, R.Y., 2008. Nucleoplasmic mobilization of nucleostemin stabilizes MDM2 and promotes G2-M progression and cell survival. J. Cell Sci. 121, 4037–4046.

Ohnuma, S., Hopper, S., Wang, K.C., Philpott, A., Harris, W.A., 2002. Co-ordinating retinal histogenesis: early cell cycle exit enhances early cell fate determination in the Xenopus retina. Development 129, 2435–2446.

Okamoto, K., Beach, D., 1994. Cyclin G is a transcriptional target of the p53 tumor suppressor protein. EMBO J. 13, 4816–4822.

Park, H.C., Boyce, J., Shin, J., Appel, B., 2005. Oligodendrocyte specification in zebrafish requires notch-regulated cyclin-dependent kinase inhibitor function. J. Neurosci. 25, 6836–6844.

Racevskis, J., Dill, A., Stockert, R., Fineberg, S.A., 1996. Cloning of a novel nucleolar guanosine 5′-triphosphate binding protein autoantigen from a breast tumor. Cell Growth Differ. 7, 271–280.

Raymond, P.A., Barthel, L.K., Bernardos, R.L., Perkowski, J.J., 2006. Molecular characterization of retinal stem cells and their niches in adult zebrafish. BMC Dev. Biol. 6, 36.

Reynaud, E.G., Andrade, M.A., Bonneau, F., Ly, T.B., Knop, M., Scheffzek, K., Pepperkok, R., 2005. Human Lsg1 defines a family of essential GTPases that correlates with the evolution of compartmentalization. BMC Biol. 3, 21.

Riley, T., Sontag, E., Chen, P., Levine, A., 2008. Transcriptional control of human p53-regulated genes. Nat. Rev. Mol. Cell Biol. 9, 402–412.

Rosby, R., Cui, Z., Rogers, E., deLivron, M.A., Robinson, V.L., DiMario, P.J., 2009. Knockdown of the Drosophila GTPase nucleostemin 1 impairs large ribosomal subunit biogenesis, cell growth, and midgut precursor cell maintenance. Mol. Biol. Cell 20, 4424–4434.

Rothschild, G., Zhao, X., Iavarone, A., Lasorella, A., 2006. E Proteins and Id2 converge on p57Kip2 to regulate cell cycle in neural cells. Mol. Cell. Biol. 26, 4351–4361.

Salic, A., Mitchison, T.J., 2008. A chemical method for fast and sensitive detection of DNA synthesis in vivo. Proc. Natl. Acad. Sci. U. S. A. 105, 2415–2420.

Saveanu, C., Bienvenu, D., Namane, A., Gleizes, P.E., Gas, N., Jacquier, A., Fromont-Racine, M., 2001. Nog2p, a putative GTPase associated with pre-60S subunits and required for late 60S maturation steps. EMBO J. 20, 6475–6484.

Shkumatava, A., Neumann, C.J., 2005. Shh directs cell-cycle exit by activating p57Kip2 in the zebrafish retina. EMBO Rep. 6, 563–569.

Skarie, J.M., Link, B.A., 2008. The primary open-angle glaucoma gene WDR36 functions in ribosomal RNA processing and interacts with the p53 stress–response pathway. Hum. Mol. Genet. 17, 2474–2485.
Stenkamp, D.L., 2007. Neurogenesis in the fish retina. Int. Rev. Cytol. 259, 173–224.
Tsai, R.Y., McKay, R.D., 2002. A nucleolar mechanism controlling cell proliferation in stem cells and cancer cells. Genes Dev. 16, 2991–3003.
Tsai, R.Y., McKay, R.D., 2005. A multistep, GTP-driven mechanism controlling the dynamic cycling of nucleostemin. J. Cell Biol. 168, 179–184.
Tsai, R.Y., Meng, L., 2009. Nucleostemin: a latecomer with new tricks. Int. J. Biochem. Cell Biol. 41, 2122–2124.
Tury, A., Mairet-Coello, G., Dicicco-Bloom, E., 2011. The cyclin-dependent kinase inhibitor p57Kip2 regulates cell cycle exit, differentiation, and migration of embryonic cerebral cortical precursors. Cereb. Cortex In press.
Watanabe, H., Pan, Z.Q., Schreiber-Agus, N., DePinho, R.A., Hurwitz, J., Xiong, Y., 1998. Suppression of cell transformation by the cyclin-dependent kinase inhibitor p57KIP2 requires binding to proliferating cell nuclear antigen. Proc. Natl. Acad. Sci. U. S. A. 95, 1392–1397.
Westerfield, M., 1995. The Zebrafish Book: A Guide for the Laboratory Use of Zebrafish (*Brachydanio rerio*). University of Oregon Press, Eugene, OR.
Wienholds, E., Plasterk, R.H., 2004. Target-selected gene inactivation in zebrafish. Methods Cell Biol. 77, 69–90.
Wu, L., Levine, A.J., 1997. Differential regulation of the p21/WAF-1 and mdm2 genes after high-dose UV irradiation: p53-dependent and p53-independent regulation of the mdm2 gene. Mol. Med. 3, 441–451.
Wullimann, M.F., Knipp, S., 2000. Proliferation pattern changes in the zebrafish brain from embryonic through early postembryonic stages. Anat. Embryol. (Berl.) 202, 385–400.
Zhang, Y., Wolf, G.W., Bhat, K., Jin, A., Allio, T., Burkhart, W.A., Xiong, Y., 2003. Ribosomal protein L11 negatively regulates oncoprotein MDM2 and mediates a p53-dependent ribosomal–stress checkpoint pathway. Mol. Cell. Biol. 23 (8), 902–912.
Zhang, J., Tomasini, A.J., Mayer, A.N., 2008. RBM19 is essential for preimplantation development in the mouse. BMC Dev. Biol. 8, 115.
Zhu, Q., Yasumoto, H., Tsai, R.Y., 2006. Nucleostemin delays cellular senescence and negatively regulates TRF1 protein stability. Mol. Cell. Biol. 26, 9279–9290.